FABRICATION AND CHARACTERIZATION OF LOW-DENSITY POLYMERIC MATERIALS WITH 3D MICROSTRUCTURES

by

HAKAN ARSLAN

Presented to the Faculty of the Graduate School of

The University of Texas at Arlington in Partial Fulfillment

of the Requirements

for the Degree of

MASTER OF SCIENCE IN MECHANICAL ENGINEERING

THE UNIVERSITY OF TEXAS AT ARLINGTON

DECEMBER 2015

Acknowledgements

First and foremost, I want to express my deepest gratitude to my supervisor Dr. Kyungsuk Yum, for all his useful comments and endless support through the entire learning process of my master thesis. I have been extremely lucky to have a supervisor who cares so much about my work, and who responds to my questions and queries so promptly. This accomplishment could not been possible without his experience and assistance. I appreciate his guidance and help in providing me in-depth knowledge for my research through valuable inputs and suggestions.

I am also highly grateful to Dr. Hyejin Moon and Dr. Daejong Kim, for agreeing to be a part of my thesis committee and sharing their valuable time and support.

During my two years research many friends and colleagues in the laboratory have provided their supportive thoughts on my research and professional life. Their names are Bitan Chakraborty, Umang Dighe, Emel Bolat and Ridvan Kirimli. Especially, I would like to thank Astha Jain and Amirali Nojoomi, who have been extremely supportive in my difficult times. I have acquired several experiences from discussions with them. I would like to thank them for making our laboratory such a great place to work.

I am indebted to the Ministry of Turkish National Education not only for providing the funding which allowed me to undertake this research, but also for giving me an opportunity to have a completely different cultural experience and a chance to meet so many interesting people.

Lastly, I wish to extend my sincere gratitude towards my family and my incredible wife, Fatma Arslan. Her continued support and encouragement has helped me overcome several obstacles. She has always believed in me and loved me even at my craziest moments.

Special thanks to the University of Texas at Arlington for providing me with a positive environment to learn and enhance my intellectual skills.

I would like to dedicate this thesis to all these wonderful people around me who have helped me throughout the entire process both by keeping me harmonious and helping me put pieces together. Without their support, I would not have been able to achieve my educational goals.

November 25, 2015

Abstract

FABRICATION AND CHARACTERIZATION OF LOW-DENSITY POLYMERIC MATERIALS WITH 3D MICROSTRUCTURES

Hakan Arslan, MS

The University of Texas at Arlington, 2015

Supervising Professor: Kyungsuk Yum

Low-density 3D polymeric microstructures with octet-truss and quad-truss were studied. These 3D microstructures were created with polyethylene glycol (PEG) using digital light processing technology. The mechanical properties of these materials with different relative densities were characterized in air and water. The experimental results were also compared and analyzed with the results from simulation studies. This work reveals that the material with octet-truss microstructures stand at least three times higher deformation than the materials with quad-truss microstructures. The polymeric material with internal 3D microstructures also shows a higher water absorption rate than the same material without internal microstructures.

Table of Contents

List of Illustrations

List of Tables

Chapter 1

Introduction

Rapid prototyping or 3D printing is one of the most advanced manufacturing methods. This manufacturing method has gained huge popularity due to its ability to make complex structures with variety of shapes and materials. Recently, 3D printing has been gaining attention in many areas, including automotive, aerospace, biomedical, energy, consumer goods, collectables, jewelry, home accessories, even food industry [1-5]. There are several different types of 3D printing systems available in the market these days [1, 2, 5-8].

In this study, a class of low-density materials with different microstructures was designed and fabricated using digital light processing (DLP). These structures can potentially be used in cushioning, energy absorption, filtration, packaging, biomaterial, thermal insulation, thermal shock catalyst supports due to their lightweight micro-lattice structures [9].

In this study, digital light processing (DLP) system was chosen to be used, considering its working mechanism, projection system, and cost. The DLP system works with photo-curable polymer systems. Thus, it is required to design and tune a photoactive resin based on the desired polymer (PEG in this case) with both good mechanical properties and printing resolution. The resin was made based on polyethylene (glycol) diacrylate (PEGDA) and polyethylene glycol (PEG) as oligomers.

After optimizing an acrylated PEG based ink system, subsequent 3D printing was performed using Digital Light processing (DLP). Two different structures, Octet-truss and Quad-truss structures, were printed with different relative densities and were studied at different environments. The experimental data then was further analyzed by simulation studies. Studies revealed that the Octet-truss configuration exhibited at least three times more deformation than the Quad-truss structure. Furthermore, it was shown that the relative compression stress is higher in the case of octet-truss structures, while both structures show relatively the same elastic modulus. Additionally, both structures show higher water absorption rate than solid structures.

Furthermore, experimental results show that the internal stress induced by the different swelling rates can be removed in the hierarchical structures, which can eliminate the formation of hydrostatic cracks. Finally, all mechanical properties were modeled to justify the experimental outcomes.

Other reports show the recoverability of structures under the stress and increased toughness and ductility of a group of perfect brittle materials by making hollow hierarchical structures [10-13]. In this work we study the swelling and mechanical behavior of different hierarchical structures in air and water environments.

Chapter 2

Manufacturing Methods and Rapid Prototyping

2.1 Manufacturing

The term “manufacturing" came from the latin term; manu factus which means made by hand [14]. Manufacturing is basically applying different processes or operations to make finished products from raw materials.

To get a product, the manufacturing process needs 5 M’s namely:

- Material,
- Method,
- Machinery,
- Men and,
- Money [15].

Today, this complex activity can be made easier and more accurate with help of new technologies - computers, robots or material-handling equipment [16].

Manufacturing has to meet some requirements for its successful operation. Engineer's Handbook [16] gives us some indispensable factors such as:

- The product must meet desired design and specifications.
- Use of most economical method to maximize cost cutting.
- Quality must be considered.
- Manufacturing companies should always remain proactive in the highly competitive business world.
- New technology and development must be implemented.
- Higher productivity.

There are many processes and techniques available to fabricate a component, as shown in figure 2-1.

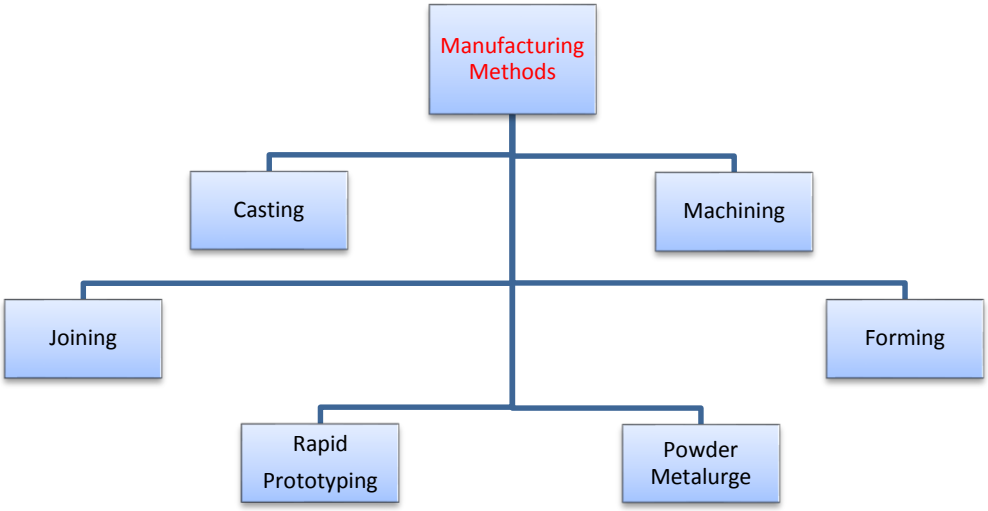

Figure 2-1 Different manufacturing process.

2.1.1 Casting

In the casting process, the solid material is heated to the right temperature, using some chemicals- until it melts. To produce desired shape and size, the molten material is poured into a mold cavity in which it keeps solidifying. Metal, plastic, glass products can be fabricated by this casting process. Some example of metal and plastic casting processes are: conventional molding processes, chemically bonded sand Molding processes, permanent mold casting, die casting, precision molding processes, centrifugal casting, blow molding, injection molding, continuous strip molding etc. [14-16].

2.1.2 Machining

The machining process or chip forming process removes unwanted material from raw work-part to get the required final shape of the product by using stationary power-driven machines. These machines use sharp cutting tools to cut away the material to achieve the final

geometry [14-18]. For performing these machining processes, the industries in US alone spend more than $100 billion every year [18].

Some examples of these processes are: turning, milling, drilling, shaving, grinding, polishing, lapping, honing, buffing, and sawing [14]. These machining process uses various machines such as lathe, shaper, and planer, milling machine, drilling & boring, grinder, saw and press [16].

The machining is the most important of the basic manufacturing processes according to Groover [17, 18], because of the following reasons:

- Variety of work materials,
- Variety of part shapes and geometric features,
- Dimensional accuracy,
- Good surface finishes,
- Wasteful of material,
- Time consuming.

2.1.3 Joining

In this process two or more components fabricated by other manicuring processes are joined together to produce the desired size and shape of a product. Joining is one of the most common and significant manufacturing processes. There are two types joining methods, namely permanent and semi-permanent or temporary [14, 15]. While permanent joining is without damage to the product and the joints cannot be separated whereas semi-permanent or temporary joining can be disassembled quickly with no damage on the material or parts [17]. Examples of permanent joining processes include welding, brazing, soldering. Semi-permanent joining processes use nuts, bolts, screws and adhesives [15, 17].

2.1.4 Forming

The manufacturing method that has been designed to use plasticity mechanical properties of materials is essentially a deformation process [14, 18]. In the production method,

suitable force, pressure or stresses are applied until exceeding the yield strength of the material for plastic deformation (hot or cold) without deterioration of their properties [14, 15, 17, 18]. No material is removed and wasted except for cutting away unwanted regions while running that process [18, 19].

2.1.5 Powder Metallurgy

Powder is made of tiny particles of solid materials such as metal, glass, polymer and ceramics [14], when they are crushed and grounded [17]. To get the desired shape, the powders are compressed, a process called compacting [18]. It is then heated until below the melting point during a process called sintering [17], the temperature is high enough to bond each particle of the material.

The powder metallurgy is a chipless [16] manufacturing method, which allows us to use the mixing of a different kind of powders to get desired properties and shapes. This method gives very smooth finish and accurate dimensions, so after this process, the product usually does not need additional post-processing [15].

2.2 Rapid Prototyping

It is one of the newest methods which differs from traditional manufacturing methods. Rapid prototyping build 3D structures layer by layer using computer-aided design (CAD) models. This method can use various materials such as metallic, plastic, ceramic, composite, or biological materials [2].

Nowadays, 3D printing systems, also known as rapid prototyping, additive fabrication, additive manufacturing, additive processes, additive techniques, additive layer manufacturing, layer manufacturing, freeform fabrication, solid freeform fabrication, and direct digital manufacturing [2], are getting popular because they freely create 3D structures as one imagines [1].

After stereo lithography was invented by Chuck Hull (Charles W. Hull) [20] in 1986 [4], additive manufacturing started to become more accessible. Since then, the additive

manufacturing has been continuously growing and evolving. According to the 2013 Wohlers report, at the very beginning of the current millennium the use of 3D printing systems has shown an increasing trend. The usage has increased from 4 percent in 2003 to more than 28 percent in 2012 [21]. In figure 2-2, the usage trend of additive manufacturing systems is shown.

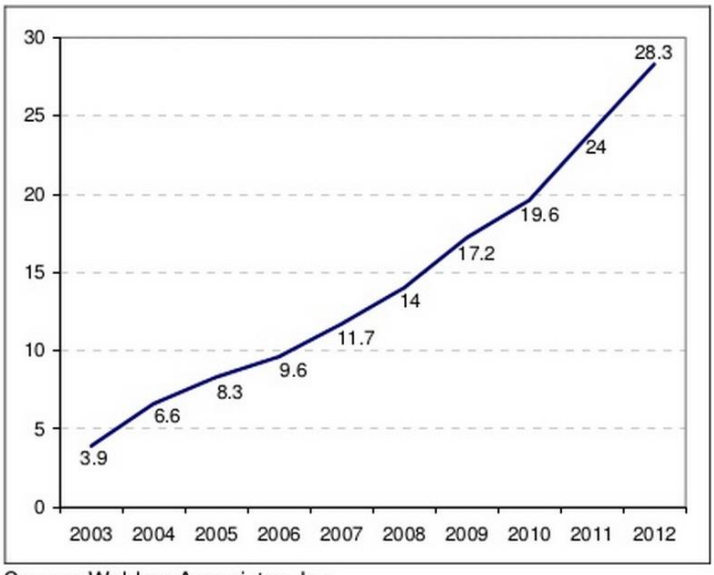

Figure 2-2 The usage trend of 3D printing systems in manufacturing processes. [21]

The 3D printing system has a wide range of applications in many industries, including automotive, aerospace, and biomedicine [1-5].

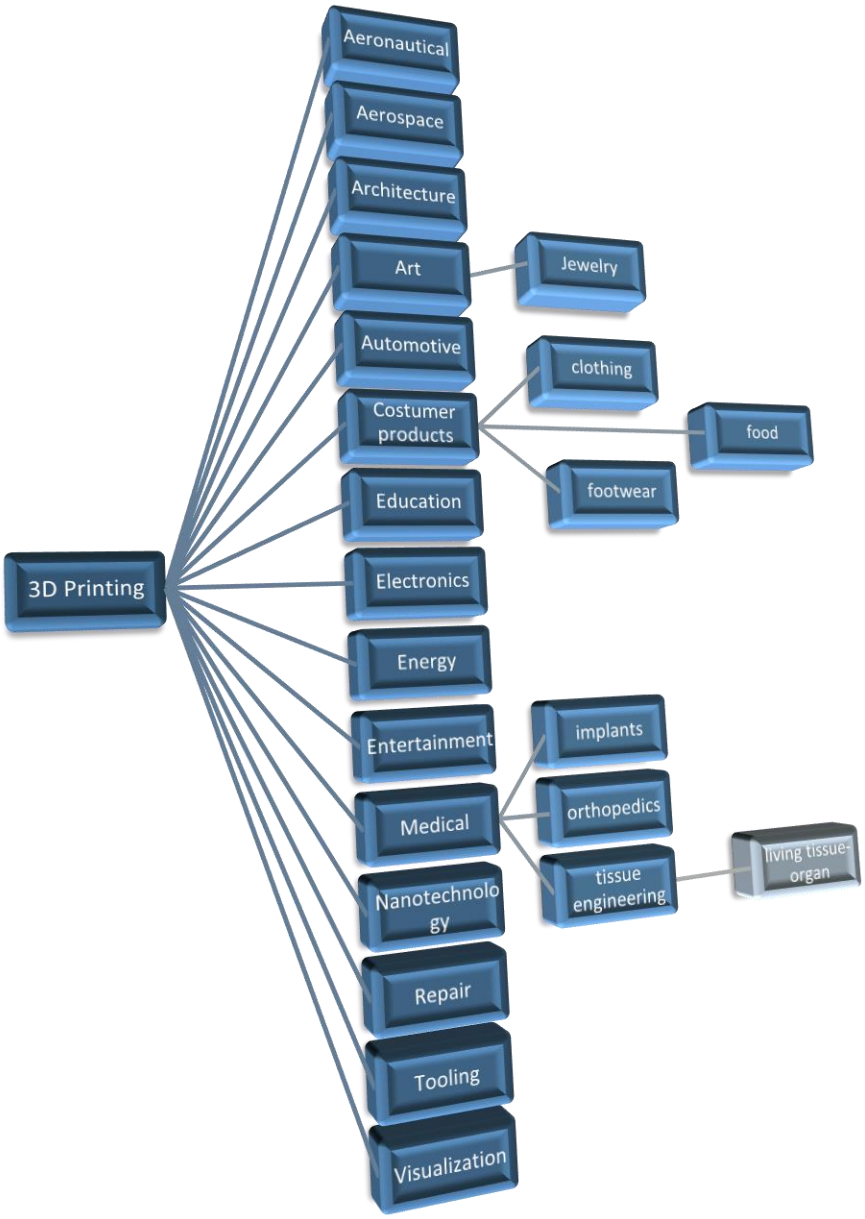

Figure 2-3 Different application areas for 3D printing systems

Chapter 3

Types of 3D Printers

3.1 Application Areas of 3D Printers

2012 Wohlers report predicts the usage of additive manufacturing (AM) technologies with a timeline from the past into the future. According to the report, between the years 2013 and 2022 nano-manufacturing, architecture, biomedical implants and in situ bio-manufacturing will become more prevalent and it is envisaged that full body organs can be printed with using 3D printers by 2032 [22].

Usage of additive manufacturing techniques is expanding into numerous opportunities every day. Aerospace parts are made of advanced materials such as titanium alloys, nickel super alloys, special steels, or ultrahigh temperature ceramics with many complex miniscule parts that can be easily manufactured using additive manufacturing. In contrast to conventional fabrication techniques these methodologies are cost effective and time saving. So, 3D printing systems are becoming more appropriate for aerospace and other similar applications. For instance, nowadays BAE Systems Regional Aircraft has started printing a plastic window breather pipe for the BAe 146 regional jetliner [2, 5, 23].

3D printers are also used in the automotive industry mainly for engine exhausts, drive shafts, gear box components, and braking systems. Making system lightweight is one of the most important factors in manufacturing racing cars which become achievable using 3D printing techniques [2, 5].

In healthcare and biomedical engineering, using rapid prototyping systems is getting more popular day by day. For example, in order to produce custom-shaped orthopedic prostheses and implants, medical devices, biological chips, tissue scaffolds, living constructs, drug-screening models, and surgical planning and training apparatuses can be easily done using rapid prototyping [2, 5]. 3D printing methods allow to customize implants and medical device according to the needs and satisfaction of patients [24].Furthermore, researchers have also tried to print

“smart scaffolds” and construct 3D printed living tissue [24], aortic valve hydrogel scaffolds [25] and ear using with bio-ink [26]. Organovo a leading 3D- Bioprinting company announced that they printed in vitro three-dimensional kidney tissue at the 2015 Experimental Biology conference in Boston [27].

Even food industry has not remained untouched with popular 3D printing and customized 3D chocolate are already available in market; furthermore, NASA has been working on a project that involves making 3D printed food for space travel that can last for long duration missions [28].

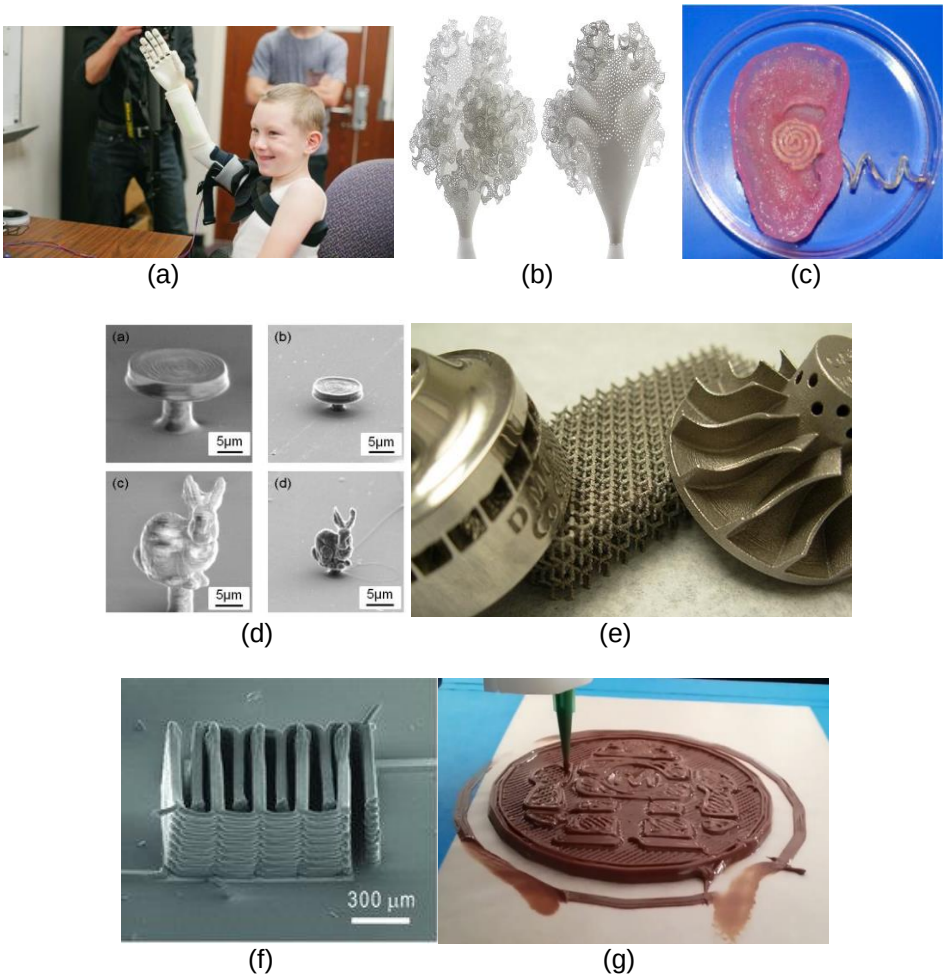

Figure 3-1 Some examples of 3D printed objects. (a) Printed prosthetic leg [29], (b) Complex 3D printed structure [30], (c) artificial printed ear [26], (d) sub-micron sized objects [31], (e) mechanical parts [32], (f) 3D Printed Li-Ion Microbattery [33], (g) 3D printed chocolate [34]

3.2 3D Printing Methods:

3D printing processes can be classified in two ways according to material used and how the system works. Categorization according to material includes three broad categories namely photopolymer, thermoplastic, and adhesives. The photopolymer uses a photocurable resin that can be solidified by its exposure to light with particular wavelengths based on resin properties. Thermoplastic system firstly melts solid thermoplastic filaments, and then the melt is cooled to get desired shape. The last system, adhesive, needs a binder for fixing to the early construction material [16].

If 3D printer systems are categorized according to their workability they can be classified as in table 3-1 below [1, 2, 5-8].

Table 3-1 Categorization of 3D Printers

Category	Technology	Material	Power Source	Example Machine
Vat polymerization	Stereolithography (SLP), & Digital Light Processing (DLP)	UV curable resin, Waxes, Ceramics (alumina, zirconia, PZT)	Ultraviolet laser, or Ultraviolet light	B9Creator, DigitalWax, CeraFab 7500
Material jetting	Multijet or Polyjet Modelling (M or P JM) & Inject Printing (IJP)	UV curable resin, Waxes	Ultraviolet Light, & Heat	Object500 Connex3, Fab@Home Model 3
Binder jetting	Indirect Inject Printing (Binder 3DP) or (BJ)	Polymers (Plaster, Resin), Ceramics, Metals, Composites	Piezoelectric Nozzle & Heat	VX Series, M-Flex, Z Printer
Material Extrusion	Fused Deposition Modelling (FDM) or Freeform Fabrication (FFF)	Thermoplastic, Waxes, Ceramics Slurries, Alloys, Metal Pastes	Heat	Replicator 2X, Choc Creator V1

Table 3-1 – *Continued*

Sheet lamination	Laminated Object Modelling (LOM) or Selective Deposition Lamination (SDL)	Plastic Film, Metallic Sheet, Ceramic Tape, Standard Copier Paper	High Power Laser & Heat	SD300Pro SonicLayer, Matrix 300+
Powder Bed Fusion	Selective Laser Sintering (SLS) & Selective Laser Melting (SLM) & Electron Beam Melting (EBM)	Thermoplastics, Metals	Laser Beam, or Electron Beam	sPro, ProX, Arcam A2
Direct Energy Deposition	Laser Metal Deposition (LMD) & Laser Engineered Net Shaping (LENS)	Melted Powder and Metal Wire	Laser Beam	Lens450, EasyClaD

3.2.1 Extrusion / Fused Deposition Modelling (FDM), Freeform Fabrication (FFF)

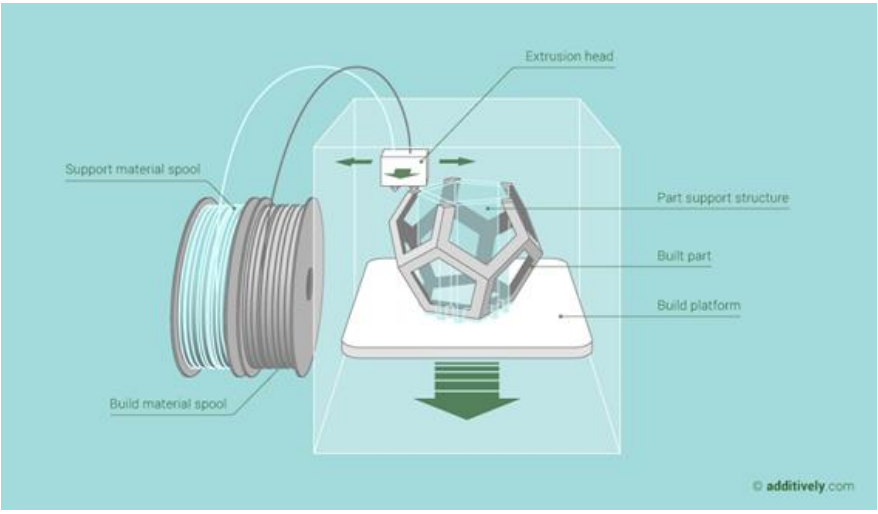

Figure 3-2 Fused Deposition Modelling (FDM) [35]

In the FDM process a thermosensitive filament, which is mostly made from ABS and PLA material, is melted then extruded through a heated extruder via a nozzle. Then, the nozzle prints the molten material on the build platform where the layer starts cooling and solidifying [6, 35].

Before starting a new layer, the previous layer gets harder and is bonded to first layer. The process continues layer-by-layer until it reaches the desired shape.

For overhanging structures, these printers need supporting materials. Selection of the supporting material is one of the most important factors on the surface quality of the printing. It is wise to choose a supporting material that is easily breakable or is dissolvable in a different solution than the final product [6].

The FDM printers and their filaments are inexpensive and the 3D printed structures durable because of good mechanical properties of the filaments [1, 6, 35]. These printers also allow the use multi-material printing. However, these machines have limited resolution, and so it sometimes causes poor and non-watertight surface finish. Acetone applications can solve problems of the printed part.

3.2.2 Material jetting

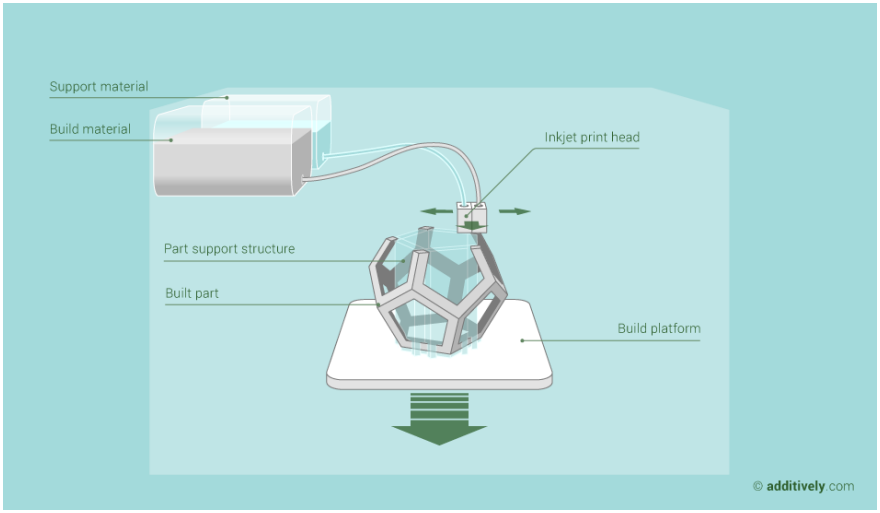

Figure 3-3 Material jetting process [35]

Inject print heads jet the wax-like or melted materials [35] towards a build table where the materials cooled and then solidified with the help of UV light and heater. The process goes on by adding one layer on top of other until the desired shape and size is obtained.

The material jetting process or inject printing system gives very accurate parts with very smooth surface finish because of high-resolution printings, and also the system supports usage

of more than one material in the same printing process [1]. On the contrary, the system has certain limitations. For instance, the final parts will be quite fragile because of usage the low-strength material, and also the used wax-like material variety is so limited [35]. The process is slow and similar to FDM printing process, supporting materials are needed for overhanging shapes.

3.2.3 Binder Jetting

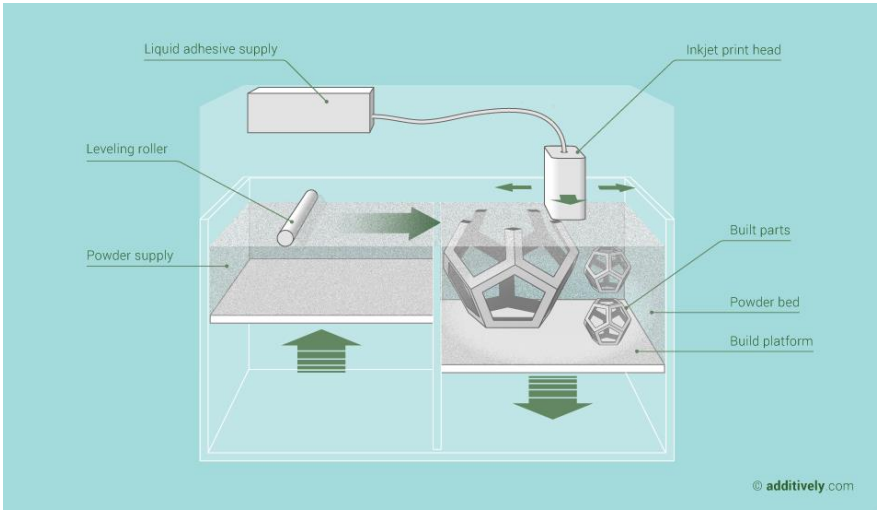

Figure 3-4 Binder jetting process [35]

The Inkjet print heads of the binder jetting machine spray a liquid bonding agent into a bed, which is filled with powder material. The bonding agent keeps the material together and forms the first layer. For the subsequent layer, the powder bed goes down (based on z-axis resolution), then another part of the printer covers the powder bed again with the material. It's built up until the powder material prints the desired shape [6, 35].

Advantages of this process include the fact that it can work with almost any powdered material including food based materials to metals. This full-color printing is a fast, simple, and cheap process [35]. During the printing process, the printed part does not need any supporting structure because the powder material supports it. However, this printing needs post processing due to the porous nature of finished parts, which requires infiltration [1] leading to weak mechanical properties (to ensure durability, usually heat is applied).

3.2.4 Sheet lamination

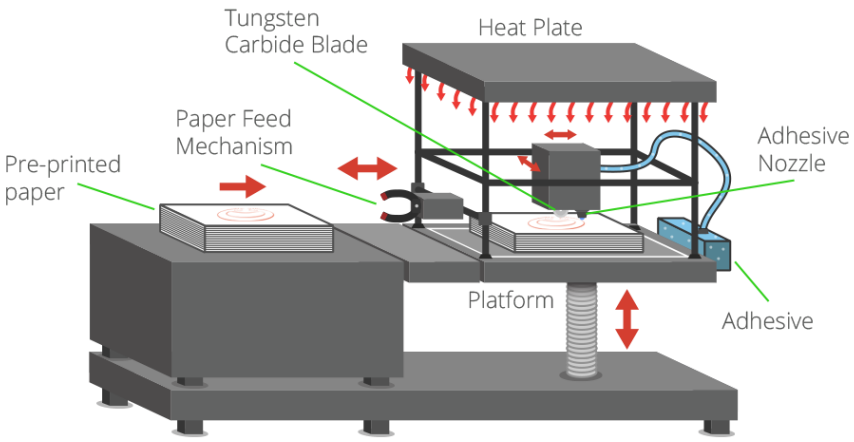

Figure 3-5 Sheet lamination process [6]

Even though this system does not seem like other 3D printers, it makes layer by layer structure by gluing each layer to the previous one. The system is supplied by a roll and the material (commonly used standard copier paper [6], but can also be plastic film, metallic sheet and ceramic tape) comes to the covered heat-activated resin/adhesive [36] platform. The layer is bonded to the previous layer because of the applied heat and pressure. Then, a blade or CO_2 laser beam cut the material to get desired shape [37]. The platform goes down in order to start a new layer. Upon completion of the entire procedure, the cut paper acquires wooden block like properties [36].

The printing system gives high surface finish and is economical due to a low cost of starting material [1]. However, in this process there is a generation of lot of unusable waste material.

3.2.5 Powder Bed Fusion

3.2.5.1 Selective Laser Sintering (SLS) / Selective Laser Melting (SLM) and Electron Beam Melting (EBM)

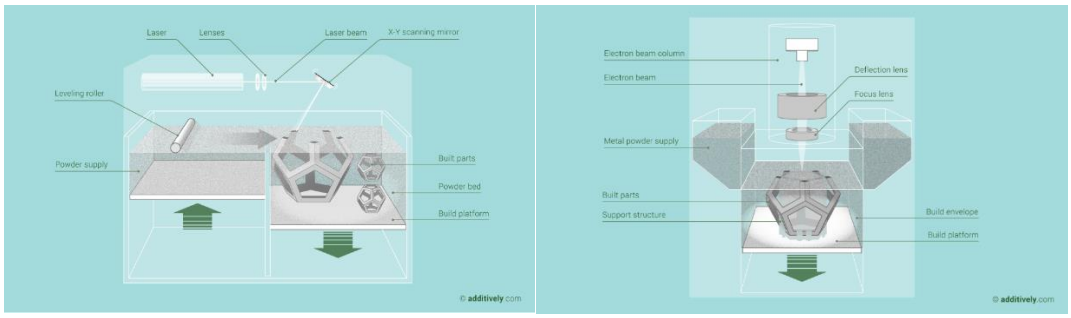

(a) (b)

Figure 3-6 Powder Bed Fusion Systems (a) Selective Laser Sintering and Selective Laser process, (b) Electron Beam Melting (EBM) process [35]

Constitutively, the powdered bed systems, laser sintering, laser melting, and electron beam melting are very similar methods. But, there is one major difference between laser sintering and laser melting. While the laser sintering works with only plastics and polyamides/polymer powder, the laser melting is compatible with a polymer, metal and ceramic powder [1, 36]. The electron beam melting have the most significant difference as compared to other powder bed fusion systems which is of thermal source as electron beam, but others use a laser which can only melt metals (conductors) [36]. Because of the use of EBM as a thermal source system it cannot be operated in an open atmosphere.

Feed cartridge are filled with powder material, and the powder material is spread in the X-Y axes until it covers all the building area and flattened (thickness is based on z-axis resolution) by a roller [1, 6, 36]. Then, a focused CO_2 laser beam melts the powder material to give a shape, and the first layer is formed, but some materials need preheating, for the purpose an IR heater is attached with some machines [36]. For the subsequent layer, the powder bed goes down (based on z-axis resolution), then another part of the printer covers the powder bed with the raw material.

It's built up until the powder material gets printed into a desired shape [6, 35]. For EBM, there is a Powder Hopper in the system instated of a roller to feed build area [36].

This printing system has some key advantages; it gives high accuracy and fine details, fully dense parts, high specific strength & stiffness and easy powder handling & recycling [1]. Nonetheless, these systems have some needs; Selective laser sintering does not need supporting structure for printing part, selective laser melting and electron beam melting need supporter layer to anchor the overhanging structures which reduces thermal stresses and prevents wrapping [35]. These printing systems also require high operating temperature thus a longer cooling time [6], surface finish is moderate to poor and porosity is much less compared to earlier system [6, 35, 36]

3.2.6 Direct Energy Deposition

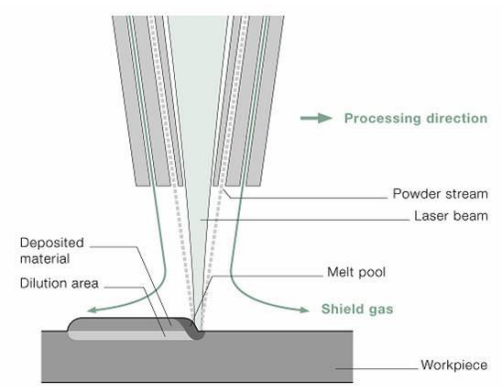

Figure 3-7 Direct energy deposition system [38]

These printing systems are called by many different names, but most of them are trademarks. For example, include Laser Metal Deposition (LMD), Laser Deposition Welding and Powder Fusion Welding, Direct Laser Deposition (DLD), Laser Engineered Net Shaping (LENS), Direct Metal Deposition (DMD), Laser Cladding [38]. These systems are very similar to the powder bed fusion and the only difference is feeding powder material to build area. Metallic powder or wire is melt by laser beam or electron beam into the focal point in order to make a melt pool [1, 38]. The build table moves x-y axis, the laser and nozzle moves in z-axis

The most significant advantage of these systems is the final products achieves 99.99% of the theoretical density of the given material [1]. The systems allow to print large parts and can be used to repair expensive parts, such as jet engine component. But, its power consumption is high due to its huge size and requires some post-processing steps [39].

3.2.7 Vat Polymerization

3.2.7.1 Stereolithography (SLP) and Digital Light Processing (DLP)

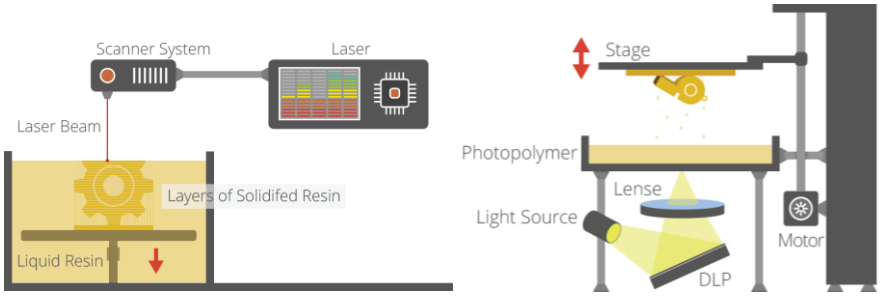

(a) (b)

Figure 3-8 Vat Polymerization (a) Stereolithography (SLP), (b) Digital Light Processing (DLP) [6]

One of the widely known Stereo lithography (SL) is laser photolithography [37] which was the first commercial 3D printing system [6]. It uses a vat that is full of photopolymer resin on the movable platform. A laser exposes UV light throughout the surface of the resin to cure (solidify) the first layer of a part. Before starting the next layer the movable platform goes down along z-axis, these going is called z-axis resolution and determine each layer thickness. These layer by layer printing continues to achieve the final structure.

Most of the application requires supporting structure such as overhangs or undercuts parts. Because of that the printed parts needs an additional post-processing step. The supporting structures can be removed manually and the structure can be easily cleaned from the uncured resin. Based on resin properties, sometimes it needs more light exposure or heat to reach desired hardness [6].

Stereolithography is one of the most accurate printing systems. The printer can achieve very high-quality finish, details and good resolution with high processing speed [1, 35]. For the printing only photosensitive materials can be use which limits the applicability of the system. Also, the cost of the material and equipment is generally expensive [1, 35].

Another vat polymerization system is Digital Light Processing (DLP). Basically Stereolithography and DLP printers are the same except for light sources. While DLP uses the more conventional light source, SLP works with an only laser beam. Moreover, the DLP printer can print in a shallow vat, so needs much less amount of resin (top-down DLP systems). In chapter 5, DLP machines are discussed in more detail. In figure 3-8 shows us the working principle of these printers.

3.3 Advantages and disadvantages of 3D Printing Systems

The rapid prototyping system or commonly known as a 3D printing process, which is distinctly different from other traditional manufacturing processes, has several advantages. The system uses the raw material more efficiently [8], reducing wastage [2, 3]. The 3D printer does not need any extra special tools or molds as compared to traditional manufacturing techniques [2, 3]. It can be used to create from easy to complex designs [3, 8]. For individual parts it is both time and cost efficient and allowing multi-material and heterogeneous composition usage [2].

However, there are some critical barriers in the 3D printing systems. Generally, the printing size is very small and the printable material is limited. They are also slow (sometimes for even a small part, the process takes several hours) [3, 40]. Moreover, the printers and their accessories, filaments and resins are not cheap [8, 40] and their maintenance is not easy [40]. In addition, the quality of product and finishing is sometimes less perfect [3, 8]. Using these system also requires skilled and experienced labors [3].

Chapter 4

Metamaterials

In nature there are many examples that are made up of cellular structures, such as trabecular bone, plant parenchyma, honeycomb and sponge, which combines lightweight with superior mechanical properties [10]. These forms inspired researchers to create biomimetic designs that make use of the lightweight structures for energy absorption, filtration, biomaterial, thermal insulation, catalyst supports and so on.

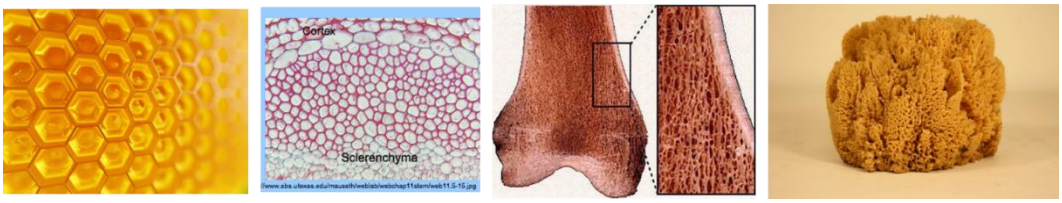

(a) (b) (c) (d)

Figure 4-1 Some examples porous structures found in nature (a) honeycomb, (b)plant parenchyma (c) trabecular bone, (d) sponge

If a solid structure is converted to a foam-like structure, almost all mechanical properties of the structure will be affected. Properties like strength, stiffness, electrical resistivity, thermal conductivity and diffusivity might all change manifolds [9]. However, the key feature might be an improvement of the mechanical properties of hierarchically ordered micro or nano-size building blocks. In nature, micro- and nanoscale building structures have random porosity that results in weak mechanical properties [10].

Before analyzing the mechanical properties of the cellular structure, mechanical properties is divided into two main categories: a stretch-dominated and a bending-dominated [9]. While the stretch- dominated cellular structures are strong and stiff based on its mass, the bending-dominated shapes are not as strong as the stretch-dominated parts, but they can absorb energy when compression is applied. In bending-dominated structures, stiffness and strength

play a less important role. Stiffness and strength play a major role in stretch-dominated triangulated lattice cellular shape [10] under application of load [41].

The principle of cellular properties depends on three main factors

I. Material properties of the cellular structure

II. Cell topology (how struts are connected) and shape of the cell

III. Relative density of the structure (ρ/ρ_s, where ρ is the density of cellular structure and ρ_s is density of solid structure of cellular shape)

As illustrated in figure 4-2, a combination of these three factors creates the properties of the cellular shape. If we elaborate more these concepts, the first factor is related to mechanical properties of the material, such as strength, stiffness, electrical resistivity, thermal conductivity and diffusivity. The second factor is related to the geometry of the cellular structure. The design must meet the Maxwell criterion; so we have to decide whether to design bend-dominated or stretch-dominated cellular structure. The final criterion is fulfilled by changing cell struts length and their wall thickness to get optimal relative density.

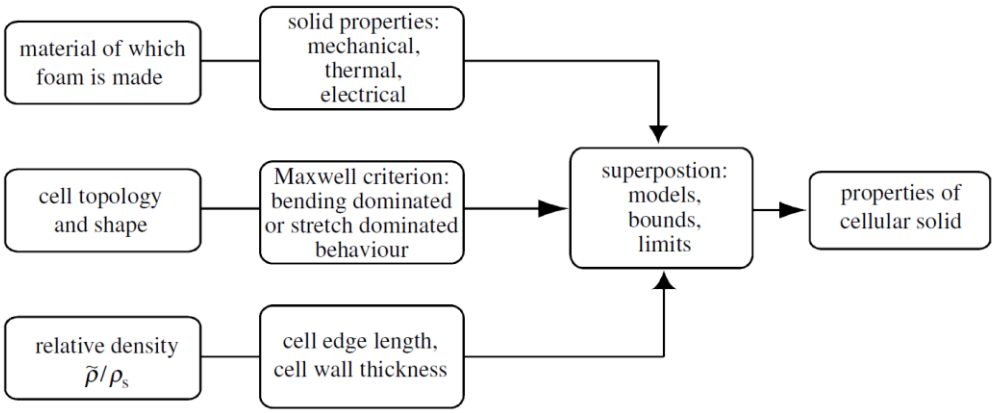

Figure 4-2 Factors of how to reach the optimal cellular structure [9]

4.1 Lattice Cellular Structure

The term lattice is defined as “a hypothetical grid of connected lines with three-dimensional translational symmetry” [9]. Nowadays, stretch dominated lattice architecture has been designed to get strong, stiff, lightweight, and recoverable nano/micro size lattice [10]. For

the mechanical metamaterials, their geometry is the most important aspect for their functionality as they are made up of highly hierarchically ordered lattice with structural connectivity in an isotropic regime.

The lattice concept actually is not a very new concept. Researchers have been working on similar lattice based structures for a long time. Previously, it was thought that these cellular properties vary linearly with relative density (ρ/ρ_s, where ρ is the density of cellular structure and ρ_s is density of solid structure of cellular shape).

After the 1960s, the concept was understood in more detail. For understanding cellular structure, Cellular Solid, which is written by Gibson and Ashby in 1997 is a masterpiece [42]. In more recent work, Zheng et al. [10] and Meza et al. [11, 13] show us how the metamaterial structure and their mechanical properties are correlated. A simple change in wall thickness, can make brittle material like ceramic to become ductile in behavior.

4.2 Maxwell's stability criterion

The configuration of a shape's edge determines if the structure can stand to bend or stretch as low strut connectivity shapes have low stiffness. To strive to find parts that have better mechanical properties, the idea of micro/nano truss lattice was presented by structural engineers. All micro/nano lattice structure should follow Maxwell's stability criterion [43], which suggests stability criterion by using an algebraic rule. The criterion can be applied to 2D and 3D shape objects.

$M = b - 2j + 3$ (2-D)

$M = b - 3j + 6$ (3-D)

Where, 'b' is the number of struts and 'j' is the number of frictionless joints [9, 10, 41, 44]. We can consider the three possibilities, (a) $M<0$, (b) $M=0$ and, (c) $M>0$.

For, $M < 0$, the structure is bending-dominated shape, so when load is applied, the shapes collapse and struts start to rotate because of low stiffness and strength [41].

For, M = 0, stretch-dominated structure, so when load is applied, the shape carry tension or compression. Ashby explains it as “stretch-dominated structures having high structural efficiency than bending-dominated structures” [9].

For, M > 0, when structure is over-constrained. Under force, the vertical struts are shortened and they pull the others. Thus, the structure carries the force because of balanced compression and tension. Although, there are no external loads these struts carry stress [9].

As Maxwell’s equations do not specify rigidity, Calladine [45] modified the Maxwell’s equations for 3-D:

$$B - 3j + 6 = s - m$$

where‘s’ is the number of states of self-stress and ‘m’ is mechanisms [41]. If the frame is kinematical and statically determinate, rigid ‘s’ and ‘m’ become zero. However, if the left-hand side of an equation equals zero, the number of mechanism and states of self-stress have the same value; it does not mean both numbers of mechanism and states of self-stress are zero.

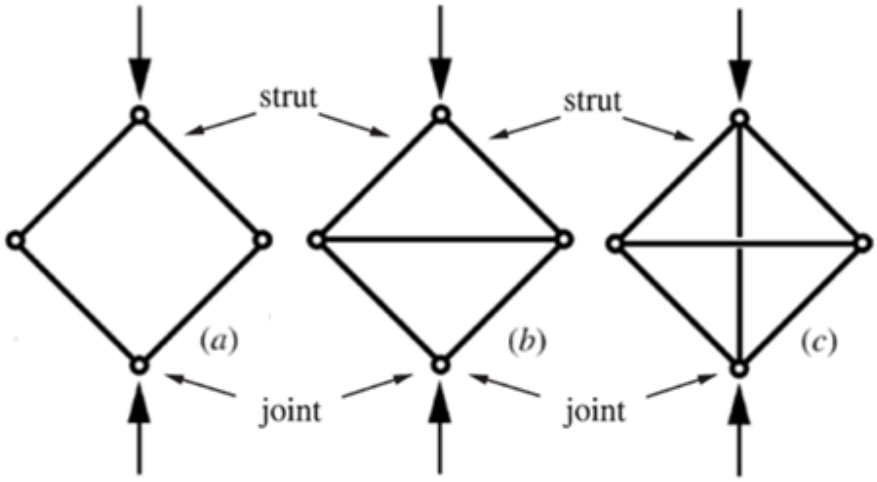

Figure 4-3 The pin-jointed frame at (a) bending-dominated structure, M<0, (b) stretch-dominated structure, M=0, (c) over-constrained structure, M>0 [9]

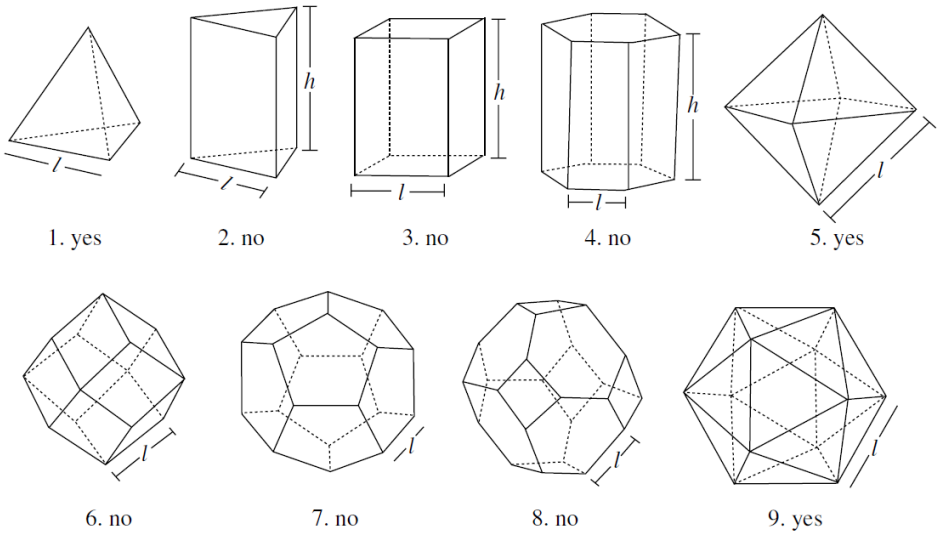

Figure 4-4 Polyhedral cells. Number 2, 3,4,6,6 and 8 are bending-dominated structures, which means M<0 [9, 41, 42]

To understand the concept of Maxwell's criterion, we can examine the above-illustrated examples. Structure 2, 3, 4, 6, 7 and 8 are bending-dominated structures, which means M<0. Structure 1, 5, and 9 are stretch-dominated lattices, which means M=0. In the following table we can see the detail of the results.

Table 4-1 For Figure4-4, Maxwell's criterion

Structure 1	M=6-3*4+6=0	M=0, so yes
Structure 2	M=9-3*6+6=-3	M<0, so no
Structure 3	M=12-3*8+6=-6	M<0, so no
Structure 4	M=18-3*12+6=-12	M<0, so no
Structure 5	M=12-3*6+6=0	M=0, so yes
Structure 6	M=24-3*14+6=-12	M<0, so no
Structure 7	M=30-3*20+6=-24	M<0, so no
Structure 8	M=36-3*24+6=-30	M<0, so no
Structure 9	M=30-3*12+6=0	M=0, so yes

4.3 Stretch-dominated structures

In figure 4-5, examples of octet-truss lattice structures, which is one the many shapes are stretch-dominated, M ≥0, are illustrated.

Firstly, if we speak of the stretch-dominated behavior, a tensile loading of the material plays a crucial role. When applying the tensile loading in the elastic stretching of the struts, approximately one-third of its struts can carry the tension regardless of the loading direction. Therefore, the relationship between relative compressive stiffness (E/E_s) and relative density (ρ/ρ_s) can be written as:

$$\frac{E}{Es} \approx \frac{1}{3}\left(\frac{\rho}{\rho s}\right)$$

where E, E_s, ρ, and ρ_s are Young's modulus of the micro/nano lattice structure, Young's modulus of the solid of which the strut is made, density of the micro/nano lattice structure, and density of the solid of which the strut is made respectively [9].

The next behavior is the plastic stretch-dominated behavior. When the applied force reaches the elastic limit, the structure yields plastically, or buckles, or fractures. Thus, the one-third of the relative density (ρ/ρ_s) almost equals to the relative compressive strength ($\sigma_y/\sigma_{y,s}$);

$$\frac{\sigma y}{\sigma y,s} \approx \frac{1}{3}\left(\frac{\rho}{\rho s}\right)$$

Where, σ_y is yield strength of the micro/nano lattice structure and $\sigma_{y,s}$ yield strength of the of the solid of which the strut is made [9].

The previous two equations are for tension or compression responses. If the structure is slender, the struts do the buckling-dominated behavior. Thus,

$$\frac{E}{Es} \propto \left(\frac{\rho}{\rho s}\right)^2$$

The magnitude of constant of proportionality can be changeable due to the connectivity of the strut [9]. However, the key factor of buckling of the structure is slenderness (t/L, where t is

the diameter of the struts and L is length of the struts), and relative density (ρ_s) regardless configuration of struts.

If the micro/nano lattice structure is made of a brittle material such as ceramic, the lattice will be failed when the applied tension or compression reaches the critical point because then these struts have stretch–fracture-dominated behavior, and start to break.

$$\frac{\sigma cr}{\sigma cr,s} \propto \left(\frac{\rho}{\rho s}\right)$$

Where σ_{cr} is critical stress of struts and $\sigma_{cr,s}$ is critical stress of material [9]. Then, the material and structure start to fracture. These cracks can exist randomly and we cannot say implicitly each fracture triggers others. For the same relative density Young's modulus and initial collapse strength of bending-dominated structures are much less than those of stretch-dominated micro/nano lattice structure. That is why the stretch-dominated structures are selected to make lightweight structures.

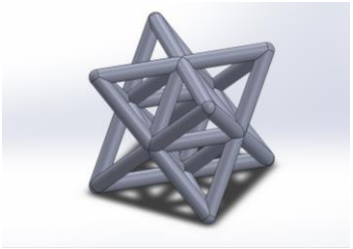

(a) 1 x1 octet-truss unit cell

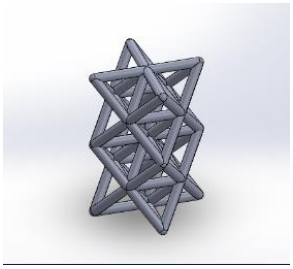

(b) 2 x 1 octet-truss structure

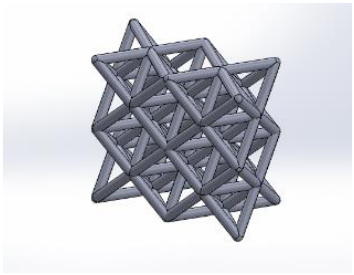

c) 2 x 2 x1 octet-truss structure

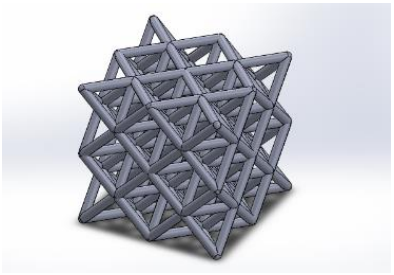

d) 2 x 2 x2 octet-truss structure

Figure 4-5 Examples of octet-truss structure with variable number units to show more than one octet-truss units is over-constrained structure, M>0 with a, b, c, d

4.4 Principle of Colum Buckling

Before making octet-truss structure, the principle of column buckling must be considered because with applied maximum or critical force, slenderness or length of struts and diameter of struts can be determined. For the octet-truss structure, we can take K=0.5 because of the fixed-fixed boundary [46]. According to the principle;

$$Fcr = \frac{\pi^2 EI}{Le^2}, \qquad here \quad Le = KL \quad and \quad I = \frac{\pi r^4}{4}$$

$$\sigma cr = \frac{\pi^2 EI}{(KL)^2 A},$$

$$\sigma cr = \frac{\pi^2 E \pi r^4}{(0.5L)^2 4\pi r^2},$$

$$slenderness\ ratio, \ \lambda = \left(\frac{L}{r}\right) = \pi\sqrt{\frac{E}{\sigma cr}} \quad or$$

$$\left(\frac{r}{L}\right) = \frac{1}{\pi}\sqrt{\frac{\sigma cr}{E}}$$

where K, L, Le, F_{cr}, σ_{cr} E, A, I, λ and (r/L) are constant that column effective length factor, the length of streets, the effective length of column, critical force (maximum applicable force), critical (fracture) strength, Young's Modulus, the area of the cross-section of struts, area moment of inertia of the cross-section of struts, slenderness ratio and transition from yielding to Euler buckling respectively.

4.5 Octahedral structure analysis

Deshpande et al. [44] gives us background of the elastic analysis of octet-truss structure. For that analysis the octahedral section of the octet-truss structure is playing a role because it determines the stiffness for the octet-truss micro/nano lattice part. But, for this calculation there are some assumptions: all joints are pinned, “only axial forces are present within the struts of the

octahedral section" [47] and the geometry has isotropic properties [48]. Thus the mechanical stain matrix can be algebraically expressed

$$\begin{pmatrix} \varepsilon x \\ \varepsilon y \\ \varepsilon z \\ \gamma yz \\ \gamma xz \\ \gamma xy \end{pmatrix} = \begin{pmatrix} \frac{1}{E} & -\frac{\nu}{E} & -\frac{\nu}{E} & 0 & 0 & 0 \\ -\frac{\nu}{E} & \frac{1}{E} & -\frac{\nu}{E} & 0 & 0 & 0 \\ -\frac{\nu}{E} & -\frac{\nu}{E} & \frac{1}{E} & 0 & 0 & 0 \\ 0 & 0 & 0 & \frac{1}{G} & 0 & 0 \\ 0 & 0 & 0 & 0 & \frac{1}{G} & 0 \\ 0 & 0 & 0 & 0 & 0 & \frac{1}{G} \end{pmatrix} \begin{pmatrix} \sigma x \\ \sigma y \\ \sigma z \\ \sigma yz \\ \sigma xz \\ \sigma xy \end{pmatrix}$$

$$\{\vec{\varepsilon}\} = [C] * \{\vec{\sigma}\}$$

Where,

$$G = \frac{E}{2(1+\nu)}$$

Deshpande et al. [44] modifies the matrix

Therefore,

$$C = \begin{pmatrix} s1 & -s2 & -s2 & 0 & 0 & 0 \\ -s2 & s1 & -s2 & 0 & 0 & 0 \\ -s2 & -s2 & s1 & 0 & 0 & 0 \\ 0 & 0 & 0 & s3 & 0 & 0 \\ 0 & 0 & 0 & 0 & s3 & 0 \\ 0 & 0 & 0 & 0 & 0 & s3 \end{pmatrix}$$

$$\frac{1}{s1} = \frac{2\sqrt{2}\pi}{3}\left(\frac{a}{l}\right)^2 Es\,, \qquad \frac{1}{s2} = 2\sqrt{2}\pi\left(\frac{a}{l}\right)^2 Es\,, \qquad \frac{1}{s3} = \frac{\pi}{\sqrt{2}}\left(\frac{a}{l}\right)^2 Es$$

Here E_s a and l are the Young's modulus of solid structure, the radius and length of a strut, respectively, and for octet-truss structure relative density (ratio of density of octet-truss part to density of the solid part) is given $\bar{\rho} = 6\sqrt{2}\pi\left(\frac{a}{l}\right)^2$. Therefore,

$$s1 = \frac{9}{\bar{\rho}} Es, \qquad s2 = \frac{3}{\bar{\rho}} Es, \qquad s3 = \frac{12}{\bar{\rho}} Es$$

By following these background, some researchers try to make ultralight, ultra-stiff and recoverable after tension and compression [2, 11-13]. The basic concept of these researchers is if the strength-dominated structure is fabricated very thin wall thickness (5nm to 100nm) to get ultralow density (<10 milligrams per cubic centimeter) with the stochastic architecture. They absorb more energy and even after more than 50% strain, they can complete recovery regardless the used material how much brittle. For example, very brittle material, ceramic, may be got ductile behavior thanks to hollow hierarchical nanolattices. These kinds of structured productions can be used on aircrafts because it leads lightweight and durable structures.

Chapter 5

Experimental Processes

5.1 Selection of 3D Printer

As mention in chapter 4, there is a wide range of 3D printers. However, selection of the right 3D Pinter is the key factor for applications. For our application, a digital light processing system (B9Creator) was selected considering the following factors.

- Working mechanism of the system: The printer works as a digital light processing (DLP) system. DLP 3D printers have many advantages over other similar printer systems, such as Stereolithography (SL). The DLP printer is faster than SL, and it needs less amount of material to facilitate the printer. Hence, there is a smaller amount of waste products, reducing the fabrication cost. Furthermore, the machines can print high accuracy products with very high resolution (it supports 5 µm for Z-axis resolution, 30 µm for XY-axis resolution), so the products' finish surfaces are smooth.
- Machine cost: The machine cost is very reasonable than other. That is not a critical factor for academic research. However, the machining costs should always been take into consideration.
- Projection System: The DLP 3D printers have two kinds of projection systems namely bottom-up and top-down projection. The system has a bottom-up projection system with several advantages. In figure 5.1 (a), a top-down projector system is illustrated. Bottom-up projection systems are shown in figure 5.1 (b).

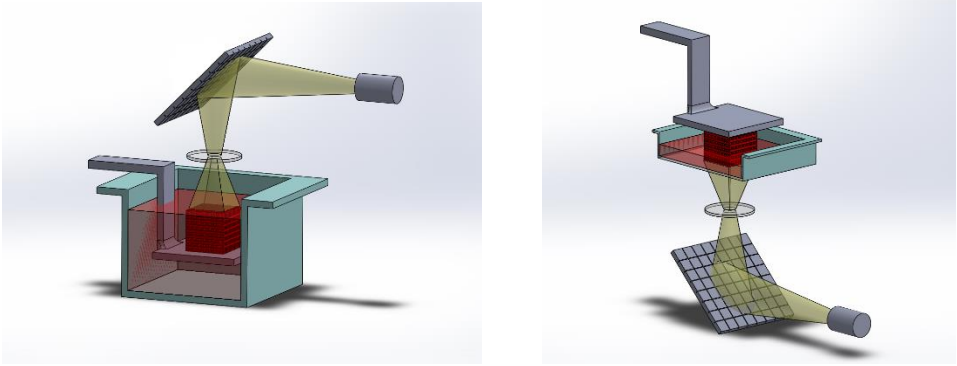

(a) (b)

Figure 5-1 Two types projection system of DLP. (a) top-down projection system, (b) bottom-up projection system

5.1.1 Advantages of the Bottom-Up Projection System

For several reasons, the bottom-up projection systems are more useful than the top-down projection systems. Pan et al. [49] make a list to show why the bottom-up projection systems is better;

1. The bottom-up systems can work with very shallow vat because after printing each layer the elevator goes up, so the depth of the container is not critical. Because of that the system needs less amount of the resin. Even if more resin required, it can be added during the process.
2. Z-axis resolution determines the thicknesses of the each layer by arranging gap size between build table, and the top surface of the vat, so fluid properties of liquid resin does not influence layer thicknesses.
3. For the top-down system, you may need to flatten the resin surface after each layer is printed, but in the bottom-up systems the resin is cured between build table and top of the vat surface. Thus, layers are more flat and accurate.

4. Oxygen-Rich environments adversely affect the cured speed. Top-Down projection systems are in direct contact with air, oxygen-rich environment. Therefore, the printing speed is slower than bottom-up systems.

5.1.2 Background

Before starting to print our sample resin, there were two critical steps to deal with: the first one is a selection of right chemicals to achieve desired properties and the second one is finding what the best composition for those chemicals.

We started to seek most commonly used chemicals, probably monomers / oligomers / polymers, cross linkers, photo initiators, and photo absorber for our applications. Polymers consist of many repeated subunits of monomers, but if the subunits are only a few they are called oligomer [50]. The cross linker assists to make a covalent bond by chemically joining two or more molecules [51]. Photo initiators are a chemical compound that can start polymerization when exposed a specific wavelengths light. Finally, photo absorbers, as we can understand from its name, can absorb light and does not let the light go into much the solution because of the characteristic more detailed parts could be printed.

After focusing on these chemicals, we decided possible candidates. Polyethylene (glycol) Diacrylate (PEGDA) or Polyethylene glycol (PEG), N,N′-Methylenebis(acrylamide) (MBAm), 2-Hydroxy-4'-(2-hydroxyethoxy)-2-methylpropiophenone - (Irgacure 2959) or Phenylbis(2,4,6-trimethylbenzoyl)phosphine oxide (Irgacure 819), and Sudan I are polymers with different molecule weights, cross linker, photo initiators and photo absorber respectively to use our applications.

PEGDA, PEG, Irgacure 819 and Sudan I were selected as the best chemicals for our study for the following reasons. PEGDA and PEG have good mechanical properties and high swelling ratios. Usage of crosslinker was avoided because it affects mechanical properties of material (it makes very hard and brittle parts). Absorption peak (around 370nm in methanol [51]) of Irgacure 819 matches our 3D printer's wavelength.

Another critical step of making our own resin is finding the best composition because even little changes in the composition yields different mechanical properties. For example, mechanical properties-strength, toughness, flexibility, and other properties like swelling ratio, response time, cure speed and resolution of 3D printed parts can be affected by changing the composition. In figure 5.2 some of the experimental results are shown in the process of finding the best composition of the resin for 3D printing. For example, before getting the optimum composition, we compared the material properties of the resin with to commercial resins as shown in figure 5-2 (a). In the following photo, to enhance material properties (mechanical, swelling and response time), SWNT (Single-wall Nanotubes) was added to the solution. But as the solution did not contain water, SWNT could not be dissolved in the solution. Figure 5-2 (c) photos shows the importance of photoabsorber in this study. The sample is very sensitive to light even when it is under the room light. When no photoabsorber was added, it was completely cured in less than 8 minutes. Figure 5-2 (d) shows some 3D printed samples.

(a) (b)

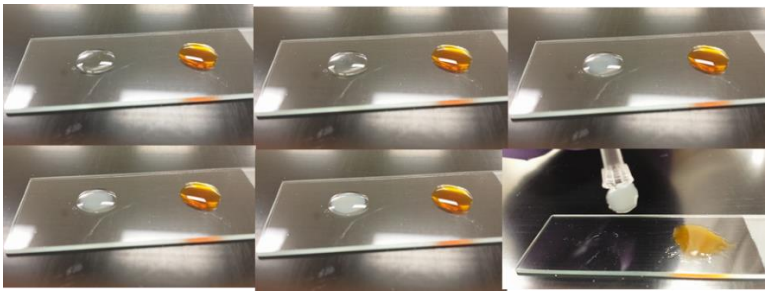

(c)

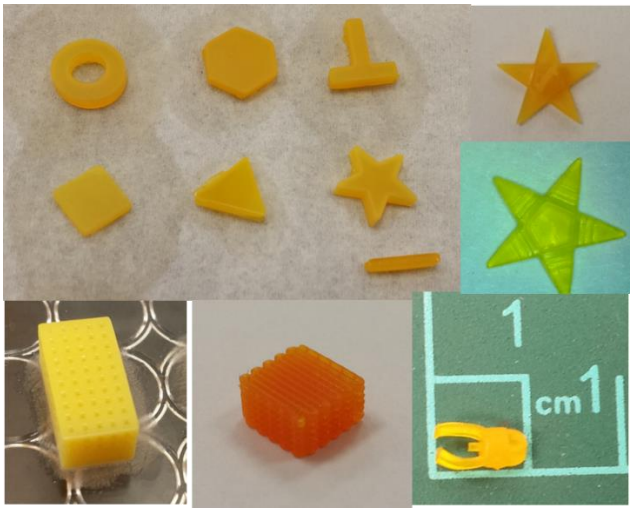

(d)

Figure 5-2 (a) comparison with commercial resins, (b) mixture with SWNT (Single-wall Nanotubes), (c) effect of photoabsorber (for 0,3,4,5,8 minutes), Some examples of 3D printed (with our own resin) parts

5.2 Analysis of the Printed Structures

5.2.1 Simulation in ANSYS

One of the most popular and accurate analysis software, ANSYS Workbench 14.0, is used to simulate mechanical behavior of our samples. ANSYS Workbench solves the problem by following fine element methods (FEM). As is known for FEM, structure is meshed with numerous points and for all these dots problem is solved. Thus, when we increase the number of dots (in a fine mesh), more accurate results are obtained but it takes much longer to solve a problem in comparison to a structure with coarse mesh because the software solves the problem for each point.

In this simulation study, 4 different set of samples with same relative densities were modeled and studied for both single-unit cell and multi-unit cell structures. These structures are solid, octet-truss and quad-truss, which are shown in figure 5-3. While running the simulation, same amount of pressure is applied on the top surface of all the structures; meanwhile the bottoms are fixed.

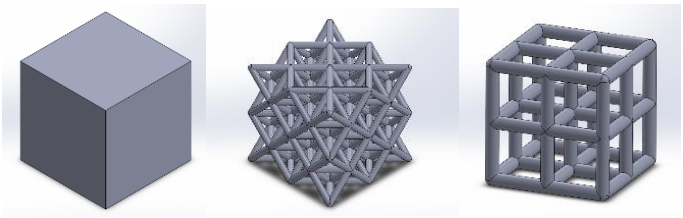

(a) (b) (c)

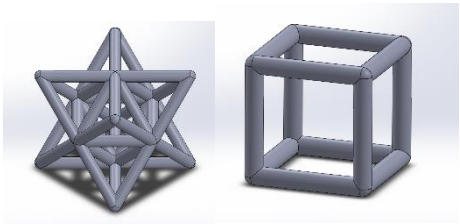

(d) (e)

Figure 5-3 Analyzed structure by ANSYS (a) Solid, (b) multi-unit cell of octet-truss, (c) multi-unit cell of quad-truss, (d) single-unit of octet-truss, (e) single-unit cell of quad-truss

5.2.2 Experiment of Compression Test

As illustrated in figure 5-4 to obtain the mechanical properties and compare to results of simulation experimentally, weight-bearing compression test was performed in two different environment – in the air and water for solid, multi-unit cell of octet-truss, and multi-unit cell of quad-truss structures.

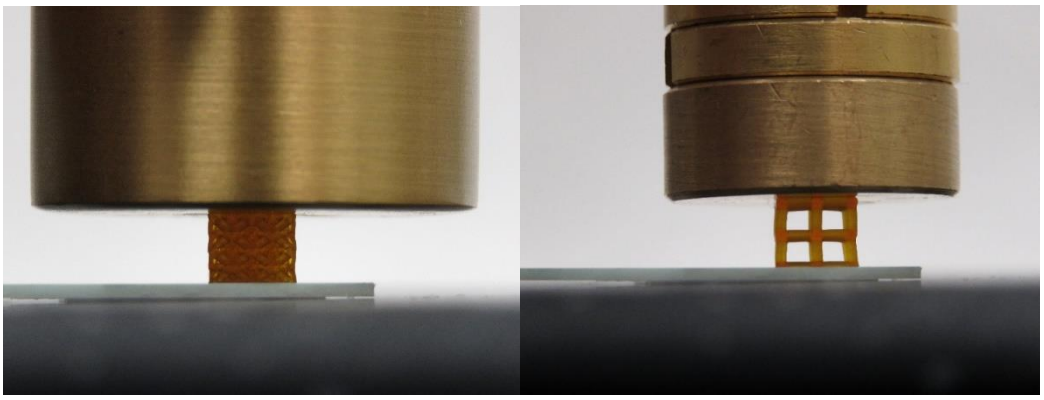

(a) (b)

Figure 5-4 Weight-bearing compression test for different cellular structures (a) octet-truss, (b) quad-truss

5.2.3 Swelling Test

For the swelling test Polyethylene glycol (PEG) based solid, octet-truss, quad-truss structures were used. We studied the swelling ratio of these structures upon one hour incubation in liquid environment at room temperature. Measurements were done every 10 seconds using digital camera (FMA050) equipped on AmScope SM-3TZ-54S-9M Digital Professional Trinocular Stereo Zoom Microscope.

All these experiment parts are discussed in detail in chapter 6.

Chapter 6

Results & Discussion

6.1 Printing

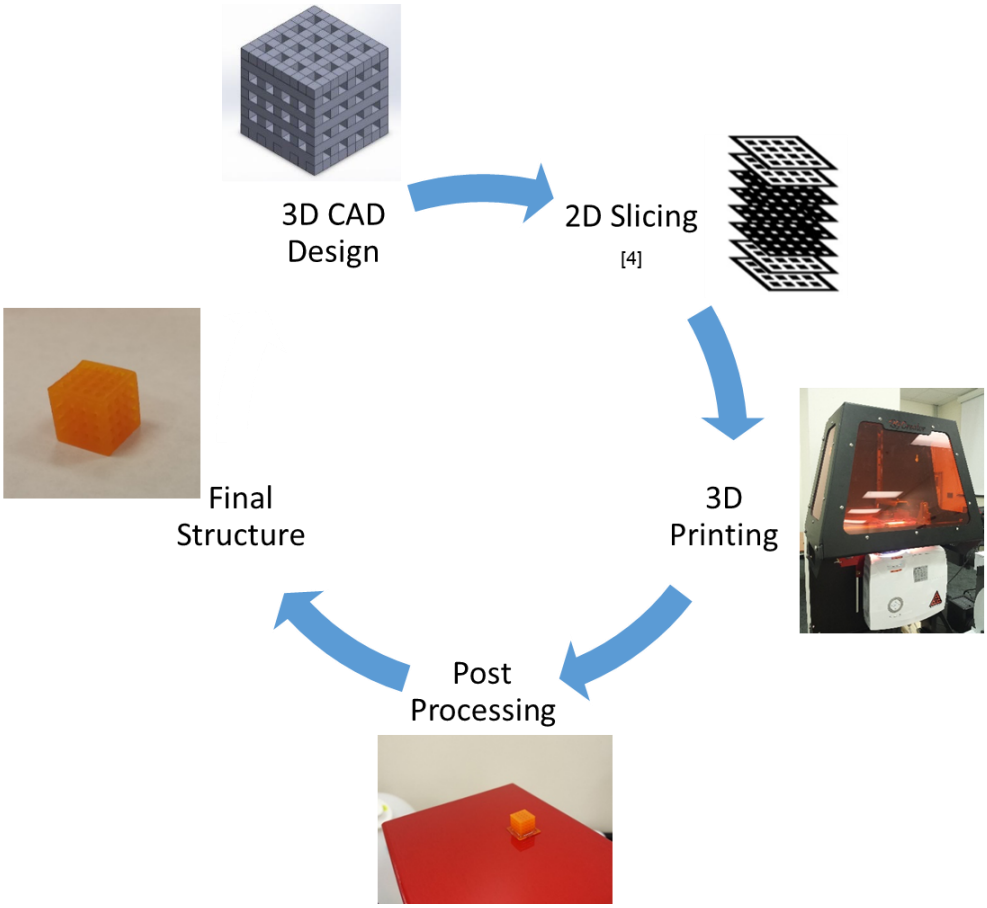

Figure 6-1 Flow diagram of my project

As shown in figure 6-1, this process starts with drawing a CAD design using a 3D CAD design software, SOLIDWORKS 2015 x64 Edition which is then saved as .STL file format as all 3D printers can work with this file format.

In order to print the structure, it must be sliced. As mentioned in chapter 2, these kind of printers expose one layer at a time, so each layer must be specified to the machine. For this step, we need to use the printer company's software, B9Creator Version1.8.0.

After this step, in order to print our samples, the resin solution should be ready. If not, the solution has to be made with the followed best composition. The best composition is given for our application in the table 6-1 and the composition is same with Lee et al. [52]. The solution is stirred at 500 rpm for 30 minutes before printing in order to prevent pellet or undissolved materials.

Table 6-1 Material Composition (%)

PEGDA (575)	PEG (200)	Sudan I (PA)	I819 (PI)
33.09	66.18	0.05	0.67

Precautions:

- When a new solution is made, the preparation is done in a dark environment, and the last chemical in this sequence should be I819 because the photo initiator is very sensitive to light.
- Before printing we always need to check if the vat is clean or not. If not, the vat should be cleaned very carefully. Firstly, the PDMS surface of the vat can be cleaned up with acetone dropped a paper towel. We should spray and wash the window of the vat (clear transparent part) with only distilled water and then dry the vat with microfiber fabric or very soft fabric. Alcoholic agents should not be used for cleaning the vat because these can damage vat leading to cracks on the acrylic sheet. Moreover, the vat should be cleaning steps should be done gently because the surface can get scratched easily.
- We use pressurized filter air to dry and remove tiny particles from the vat.
- It should not be forgotten to take the PEGDA resin out on the stirrer and keep it undisturbed for 10 minutes to remove air bubbles inside of the resin.
- If the printer is not calibrated, it should be done before starting to use it. However, before each printing process, it is suggested to calibrate both the projector and building table.

- If calibration is required, you need to follow the instructions after running software of B9Creator because it says exactly what you are supposed to do. Now everything is ready to print our structures.

When printing is completed, we need to remove the building table thumbscrew and for a while keeping it vertically in order to dribble down rest of the material in the vat. Then we need to take out the 3D printed part on the building table, and then detach the attach layer from the printed parts. These steps are critical, if not performed carefully and gently, all effort might get wasted because the parts are quite small and tend to break easily. For other post processing steps, we need to get rid of uncured resin from our structure. Thus, the structure is kept in an acetone bath for 2 hours, then allowed to dry by keeping it in an air blower chamber for 30 minutes. As a final step, the parts put on the 60°C heater for least 3 hours. After all these steps, the structure will be entirely dry, but as an optional post processing step, the printed parts can be kept at a room temperature for overnight. In figure 6-2 we can see after all steps, 3D printed micro lattice structures.

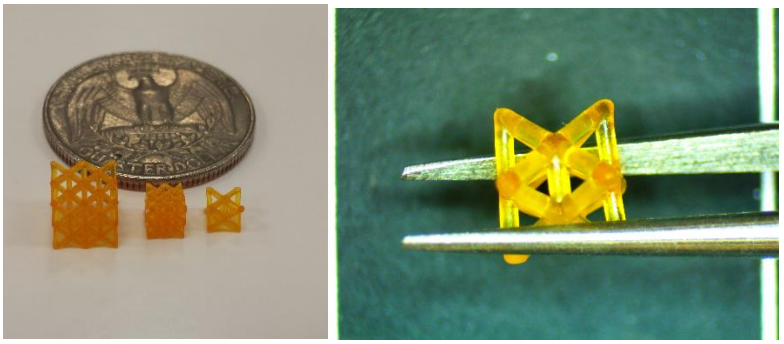

(a) (b)

Figure 6-2 (a) 2x2x2 micro lattice structure and different size unit cells (b) just unit cell of octet-truss structure

6.2 Simulation of Mechanical Properties

Before starting the simulations, all three parts, octet-truss, quad-truss and solid cube were drawn by SolidWorks2015. Octet-truss structures with the four different relative densities were designed, along with four Quad-truss structures with the same relative densities as the Octet-truss structures. Also, structures with different number of unit cells (one and eight-unit cells) were designed to study the influence of unit cell number on the behavior of the system. To decide the dimension of other structures and find out the density of these structures, the solid cube structure was used as the base. The density of the material was 1237.5 $kg.m^{-3}$. For both one-unit cell structure and eight-unit cells structures, the properties are mentioned in table 6-2 and 6-3.

Table 6-2 Different design dimensional multi-unit cells structures

Octet-truss	Mass of the structure (kg)	Volume of solid (mm^3)	Density of structure (kg/m^3)	Density of solid (kg/m^3)	Young's modulus of solid (MPa)	Relative density
8.5	0.000139	614.125	226.6477	1237.5	6	0.18315
8.55	0.000165	625.0264	264.4848	1237.5	6	0.213725
8.6	0.000193	636.056	303.4953	1237.5	6	0.245249
8.65	0.000222	647.2146	343.3482	1237.5	6	0.277453
Octet-truss						
8.92	0.00016	709.7323	224.8735	1237.5	6	0.181716
9.02	0.000194	733.8708	264.0247	1237.5	6	0.213353
9.11	0.000227	756.058	300.0828	1237.5	6	0.242491
9.22	0.00027	783.7774	344.8173	1237.5	6	0.27864

Table 6-3 Different design dimensional multi-unit cells structures

Octet-truss	Mass of the structure (kg)	Volume of solid (mm^3)	Density of structure (kg/m^3)	Density of solid (kg/m^3)	Young's modulus of solid (MPa)	Relative density
5.5	0.000024594	125	196.752	1237.5	6	0.158992
5.55	0.000029368	128.78	228.0478	1237.5	6	0.184281
5.6	0.000034486	132.651	259.9754	1237.5	6	0.210081
5.65	0.000039928	136.59	292.3201	1237.5	6	0.236218
Octet-truss						
5	0.00016	125	186.792	1237.5	6	0.150943
5.05	0.000194	128.78	207.3536	1237.5	6	0.167558
5.1	0.000227	132.651	228.1702	1237.5	6	0.18438
5.15	0.00027	136.59	249.2057	1237.5	6	0.20137

After designing the parts by the CAD program, sample were exported to ANSYS Workbench to study their mechanical properties. As the figure 6-3 shows, a same amount of pressure is applied on the top surface of all structures; meanwhile the bottoms are fixed.

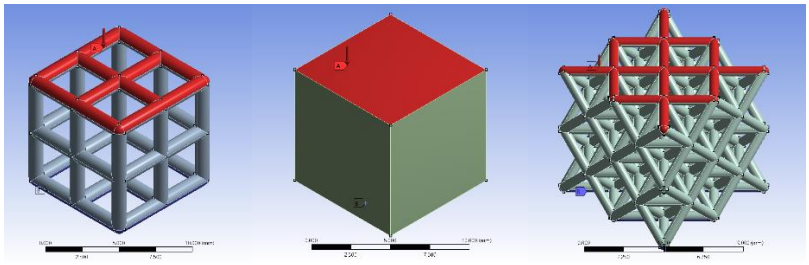

Figure 6-3 The pressure is shown as A, fixed support is shown as B, (a) multi-unit quad-truss lattice structure, (b) solid cube structure, (c) multi-unit octet-truss cells structure

To study and compare the behavior of one unit-cell and multi-cell structure, different pressures of 0.01 MPa and 0.0009 MPa were applied on the top surface of structures depending on their failure stresses. For printing and compression test, a sample group with the same relative density was selected from each multi-unit cell and single-unit cell structures to experimentally

study their mechanical behavior. To study the amount of failure strength for each structure, different pressures were applied.

6.2.1 Multi unit-cell structures

In this section, we explain the simulation results of the multi-unit cell structures (eight unit-cells) with different relative densities. Figure 6-4 shows the stress strain curve for Octet-truss and Quad-truss structures with the same relative density. Although both structures show relatively the same Young's modulus, the Octet-truss structure shows higher compressive strength and ultimate (Failure) strain.

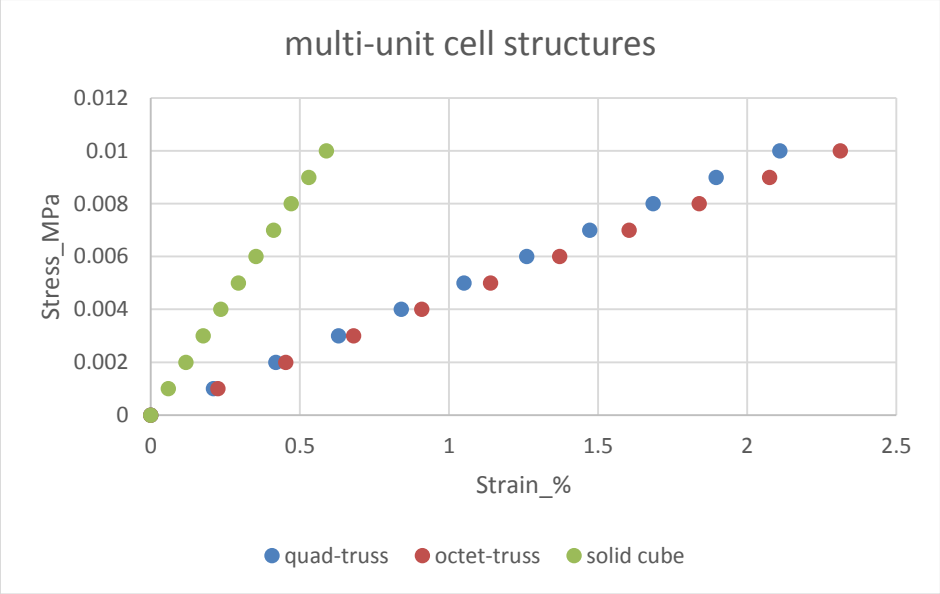

Figure 6-4 0.01MPa Ultimate pressure was applied on the three parts

Simulation results show that the compressive strength for the octet-truss structure is three times more than the Quad-truss structure. Moreover, the ultimate (Failure) strain at the failure point for Octet-truss structure is also about four times more than the quad-truss (Fig 6-5). The reason of this behavior can be linked to the design of the structures.

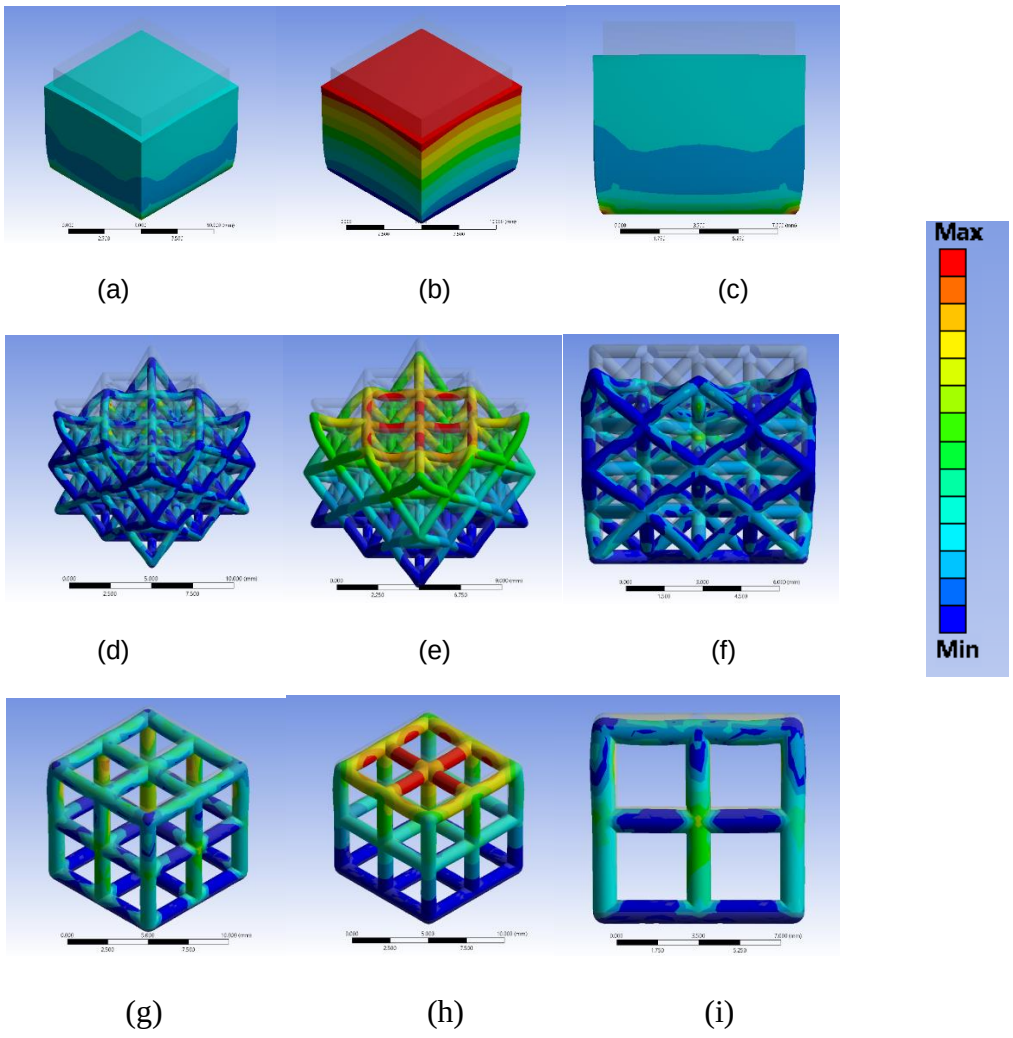

(a) (b) (c)

(d) (e) (f)

(g) (h) (i)

Figure 6-5 a,d,g are maximum stress, b,e,h, are max deformation, c,f,i are maximum strain until failure

In the case of Octet-truss structure there are enough number of struts to transmit the force, moreover, as it was explained earlier during discussion on Maxwell's stability criterion that the octet-truss structure has Maxwell number (M) which is more than zero, the structure is considered as a "Over-constrained stretch-dominated" structure. As it was explained in the section, 4-2 and 4-3, when these structures are loaded the struts carry compression which makes the slender to be under stretch condition instead of bending condition. As a result, the structure behaves much stiffer, in that, its components are under stretch instead of bending. However, in

case of Quad-truss structure, the Maxwell number is less than zero, thus, the structure has one or more degrees of freedom and if the joints are locked the bars are bent when the structure is under load. Simulations show that the ultimate compression failure stress (Figure 6-5) for the octet-truss structure is three times more than the Quad-truss structure. Moreover, the ultimate displacement at the failure point for Octet-truss structure is also about 4 times more than the quad-truss.

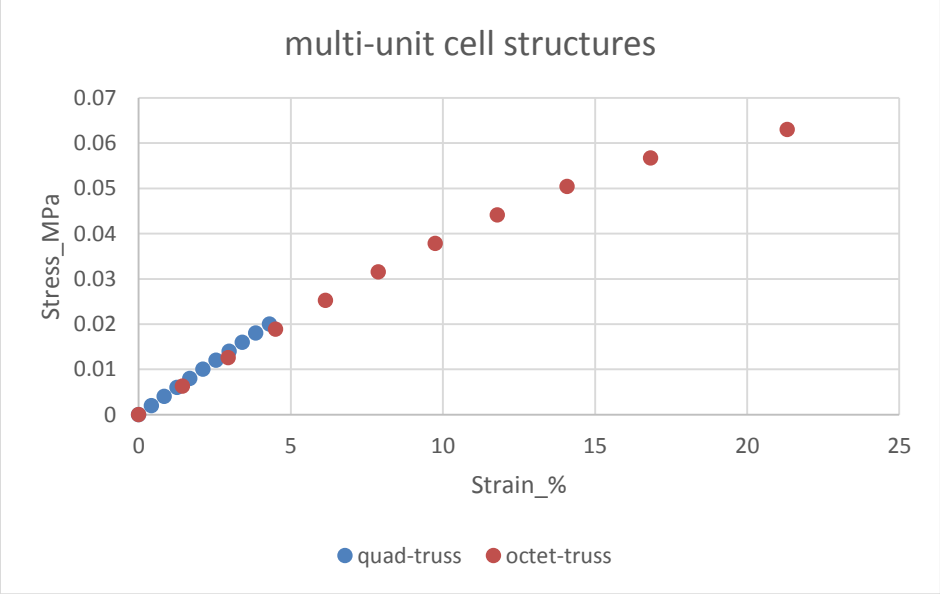

Figure 6-6 Ultimate (Failure) stress-strain curve

To confirm these results the elastic modulus, compressive strengths and failure strains for Octet-truss and Quad-truss structures with different relative densities were measured (Fig 6-6, 6-7, 6-8).

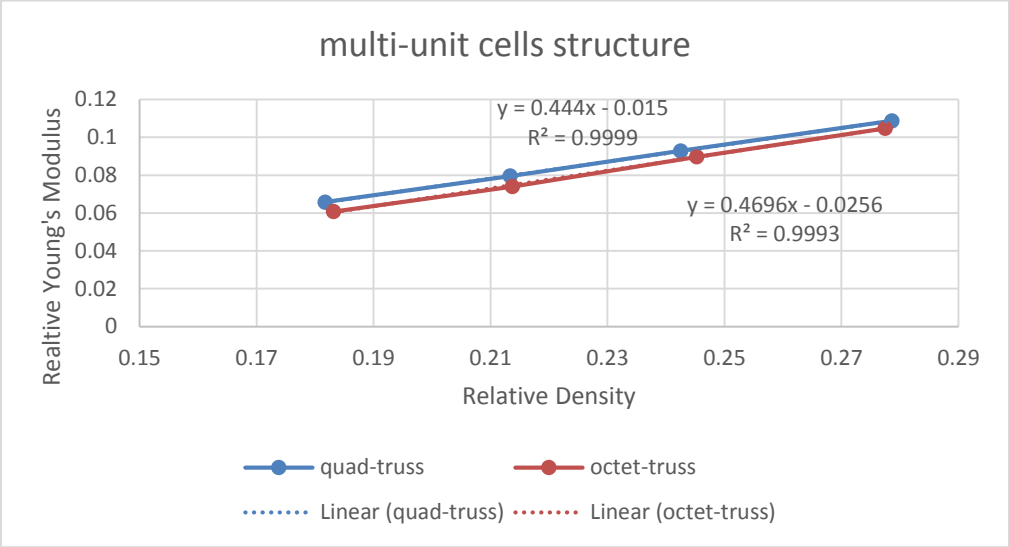

Figure 6-7 Relative elastic modulus-relative density for four different sets of multi-unit cell structures

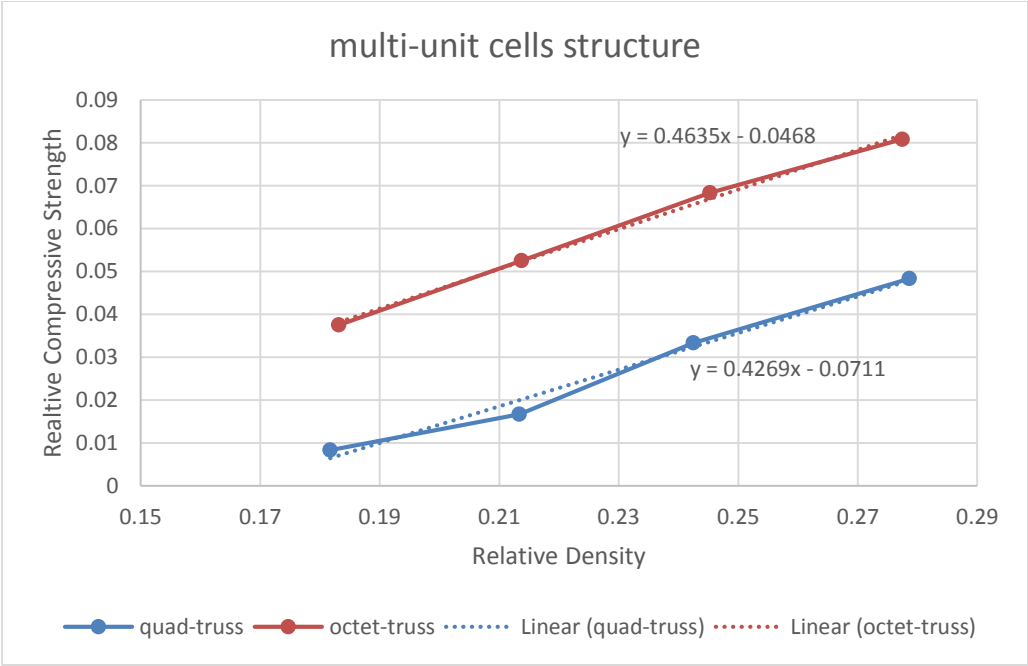

Figure 6-8 Relative compressive strength-relative density for four different sets of multi-unit cell structures

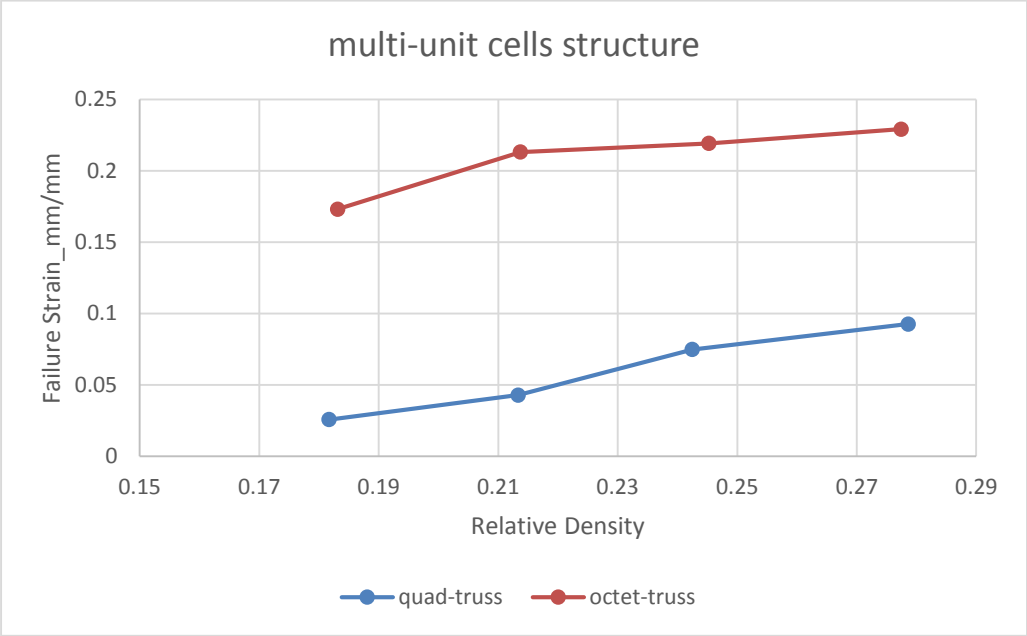

Figure 6-9 Ultimate (Failure) strain- relative density for four different sets of multi-unit cell structures

As it is shown in all aforementioned figures, the amount of compressive strengths, failure strains and especially elastic modulus increase linearly by the relative density.

6.2.1 Single unit-cell structures

Figure 6-10 shows that the single unit-cell of Octet-truss as a stretch dominated structure shows significantly higher amount of elastic modulus and compressive strength.

The behavior of the Octet-truss structure remains almost the same for both single and multiple unit cell structures.

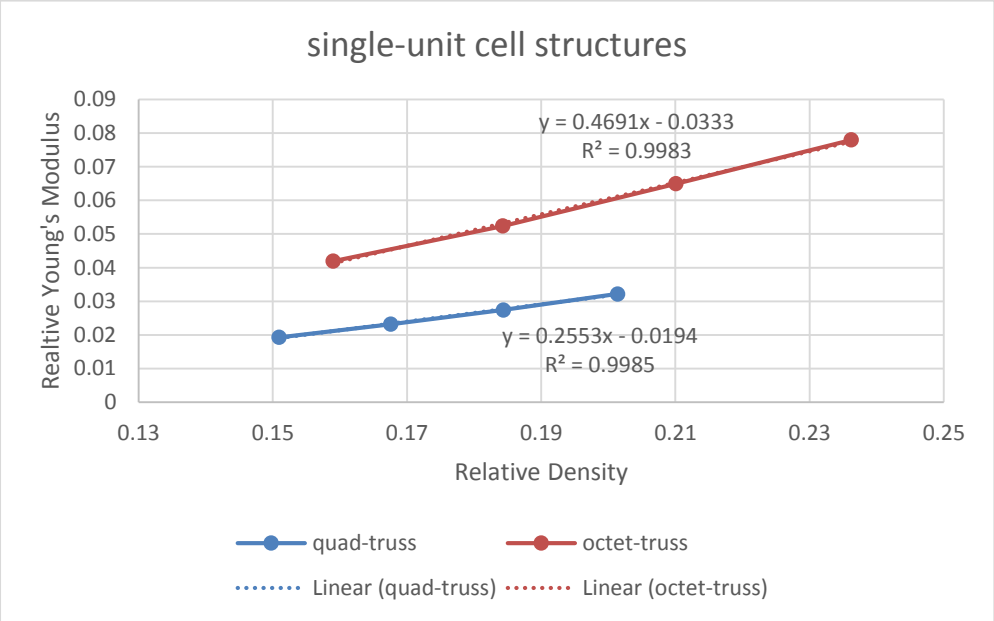

Figure 6-10 Relative elastic modulus-relative density for four different sets of single-unit cell structures

However, the quad-truss structure shows higher deformation in case of one unit cell structure which can be attributed to the nature of the observed deformation. In case of single unit-cell all four struts along the applied load will be bended leading to deformation along the z-axis, while, the nature of the observed deformation is bending of the struts. However, in case of multi-unit cells structure, due to the locked joints, the middle part of structure is stretch dominated, thus, the deformation would be limited by the compressive deformation of stretch dominated parts, thus, the deformation is compressive in nature. In this case, as it is shown in the Figure 6-11, the multi-unit cell structure shows higher elastic modulus and lower total deformation.

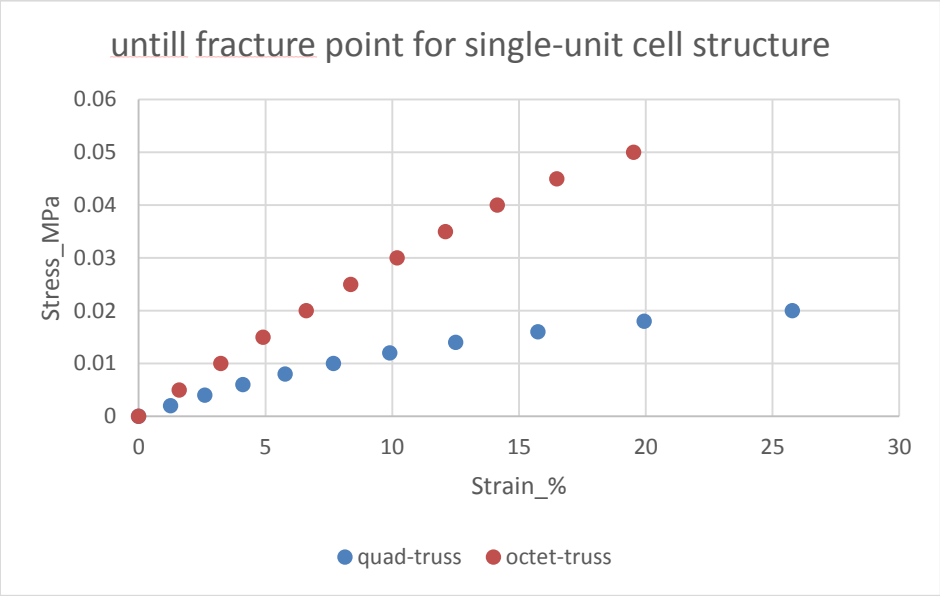

Figure 6-11 Ultimate (Failure) stress-strain curve

In figure 6-12 location of maximum stress/strain and maximum deformation distributions of the one unit cell structures.

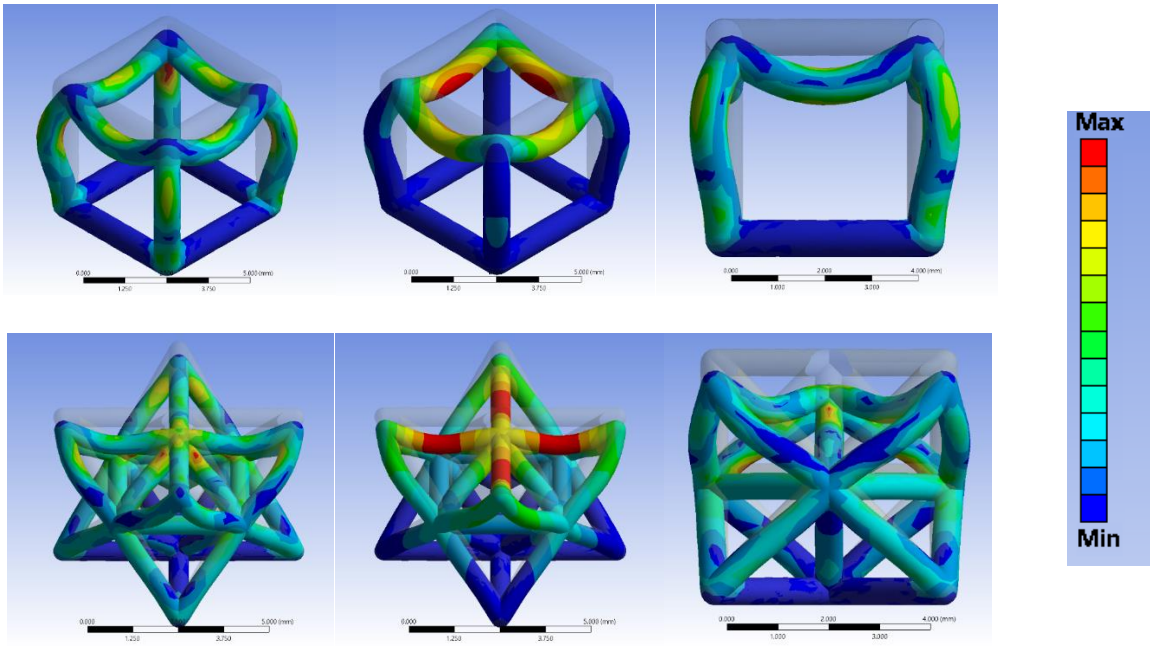

Figure 6-12 Location of maximum stress, deformation and strain

6.3 Compression Test

To obtain the mechanical properties of the multi-unit cell structure experimentally, weight-bearing compression test was performed in two different environment – in the air and water for solid, octet-truss, and quad-truss structures.

6.3.1 Air Environment

Figure 6-13 shows the obtained stress-strain diagram for the multi-unit cell structure at air environment. Experimental data shows a good harmony between the obtained experimental results and the modeling. The obtained ultimate (Failure) strain data from the experiment shows more than 90% in harmony the simulation. Furthermore, the young modulus of both octet-truss structure and Quad-truss structures are relatively the same as it was expected by the modeling data. Moreover, the obtained data from the experiment shows more than 80% similarity to acquired data from the simulation. The reason of this difference can be attribute to the post-processing steps. The post processing shrinkage can affect the dimensions, density and consequently the relative density, which is directly related to, the Young's modulus of the structure.

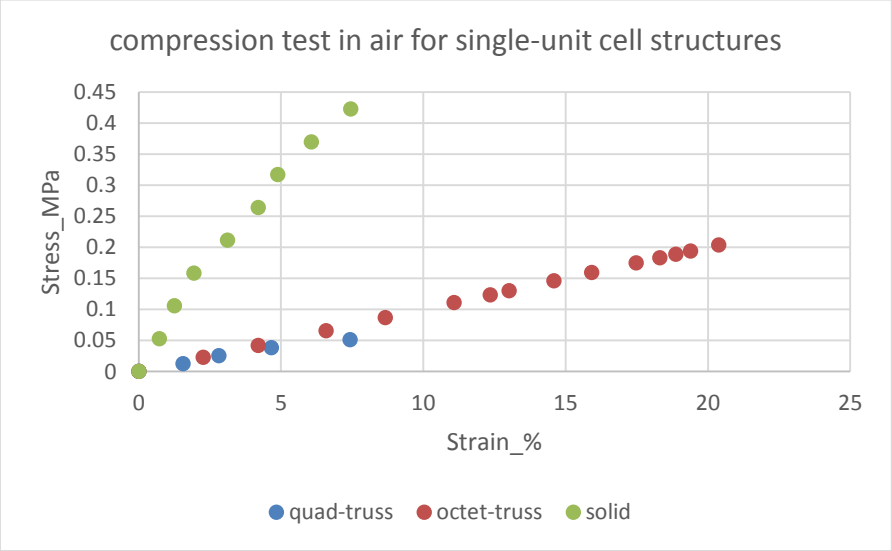

Figure 6-13 Weight-bearing compression test in air environment for each point 50 gram increased the weight

Figure 6-14 shows the shape of the octet-truss structure. Measurements show that the elastic loading is more than 90% recoverable. Also, the sample does not abruptly fail after initiation of a crack and it can also withhold subsequent higher loadings. The reason can be attributed to the ordered structure of the sample, in which, each unit cell can contribute on the load bearing mechanism separately. Moreover, there is no crack propagation in these structure due to the fact that each strand fracture separately. These properties inhibit the abrupt failure of the structure after a certain load making them reliable for engineering applications. Figure 6-14, shows the behavior of the octet-truss after the breaking point, as it appears even after crack initiation the structure remains uniform and can bear even more load.

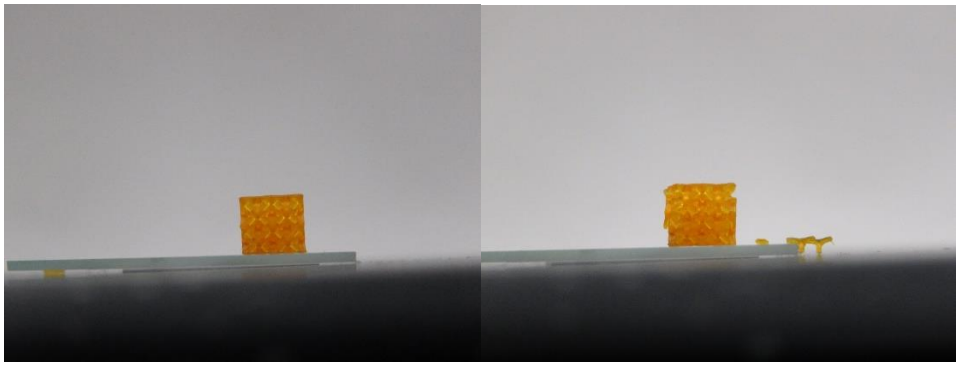

(a) (b)

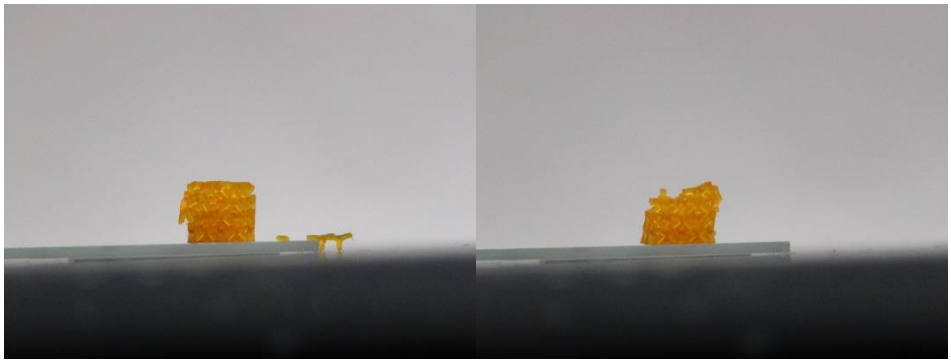

(c) (d)

Figure 6-14 Fracture propagation and recovery of the structure(a) after applied 650-gram weight and start a little crack, in the (b) after 655 gram, (c) shows after 660 gram and the final is 665-gram weight applied to see breakage and recovery.

6.3.1 Water Environment

For the water compression test, all three structures were kept in the 23 °C deionized water for 20 minutes to be fully swelled.

After swelling, these structures get more fragile and Young's modulus and stiffness decrease dramatically (the same protocol was applied, 50-gram added weigth) .In this experiment almost just half of the strain can be reached. the figure 6-15 the stress-strain curves were given for all each structure.

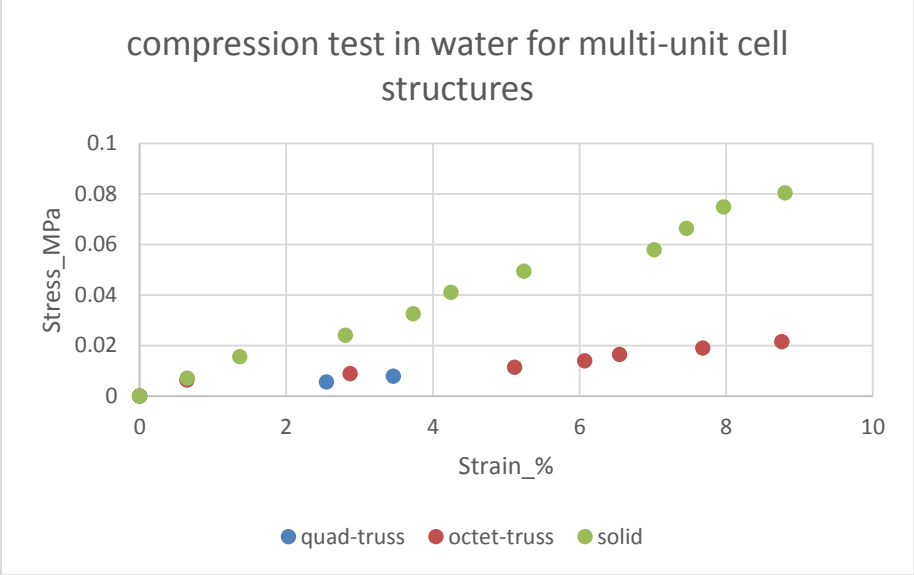

Figure 6-15 Weight-bearing compression test in water environment for each point represents 50 gram additional weight

6.4 Swelling Test

Considering the fact that these structure may be ultimately used for actuation applications, the swelling ratio is going to be one of the important aspects of these structures. To perform the experiment, the solid, quad-truss and octet-truss structures were printed with same relative density and outer dimensions. Samples were put in the deionized water at 23 °C for one hour and measurements were done every 10 seconds using digital camera (FMA050) equipped on an AmScope SM-3TZ-54S-9M Digital Professional Trinocular Stereo Zoom Microscope.

Figure 6-16 shows the swelling amount (mm, percentage) time. The same relative density octet-truss and quad-truss structures almost saturate in water with a very fast initial response.

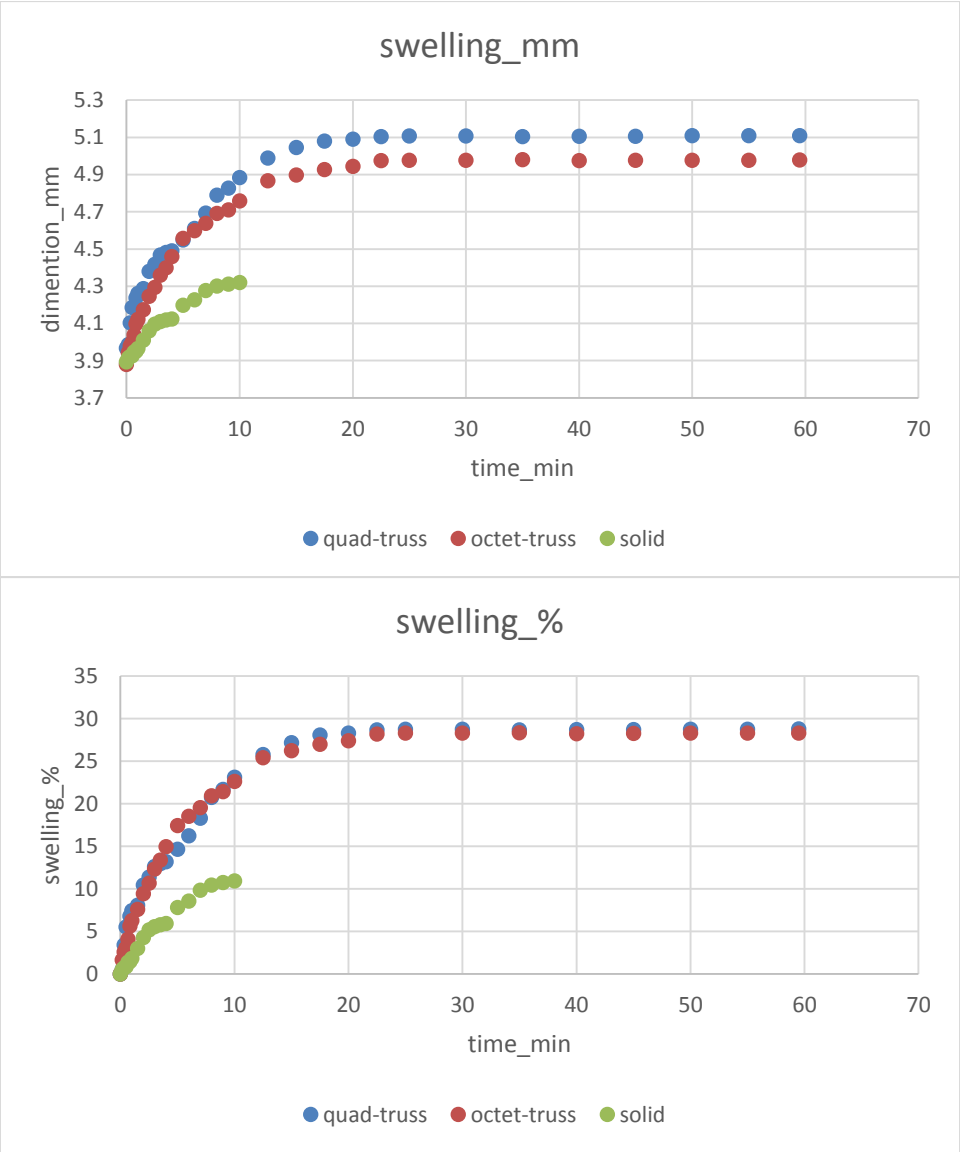

Figure 6-16 Swelling of the quad-truss, octet-truss and solid structures

However, the solid cube slowly swells, and fails prior to reaching its fully swelled state (after 10 minutes). The reason of this behavior can be pointed towards to the high difference of swelling ratio between different parts of the solid sample. Relatively low amount of water diffusion through the solid part makes the outer shell to be fully swelled first while the inner part remains

same. This excessive swelling difference between inner part and outer part induces high internal stress within the solid sample, which makes the sample breaks every time before reaching to the full swelling state (Fig 6-17).

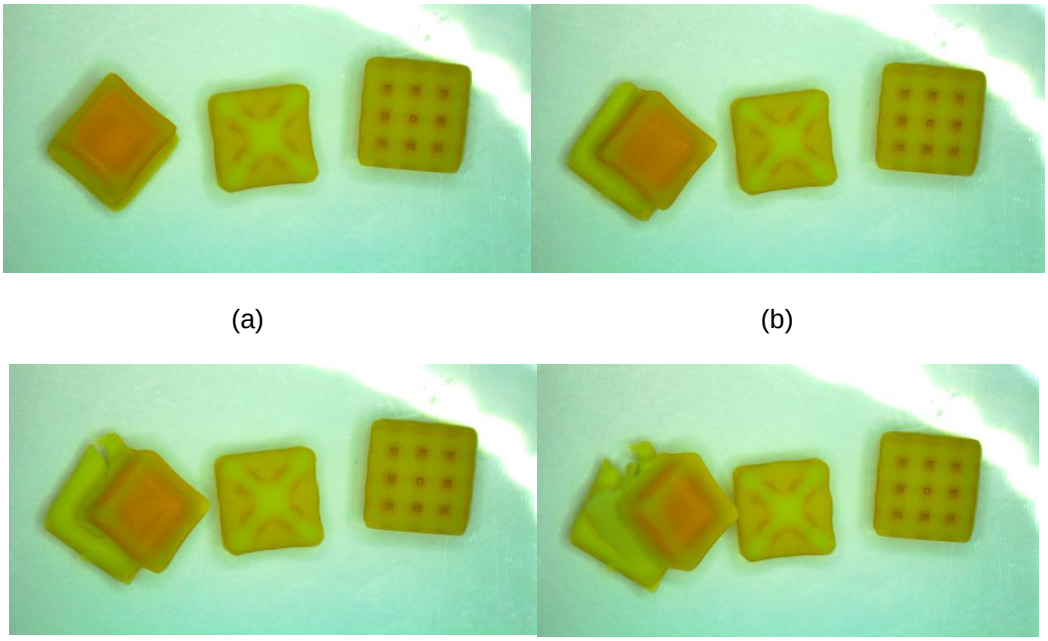

(a) (b)

(c) (d)

Figure 6-17 Breaking of the solid structure (a) 10.5 minutes, (b) 11 minutes, (c) 11.5 minutes, (d) 12 minutes

In contrast, having hollow parts for octet-truss and quad-truss structures eases the diffusion water into the structure, which leads to a uniform swelling pattern. Thus, both structures show high swelling rate and uniform swelling pattern, which prohibits the formation of internal stress due to the different swelling amount through the sample. The sample can swell approximately 30% illustrated in figure 6-18.

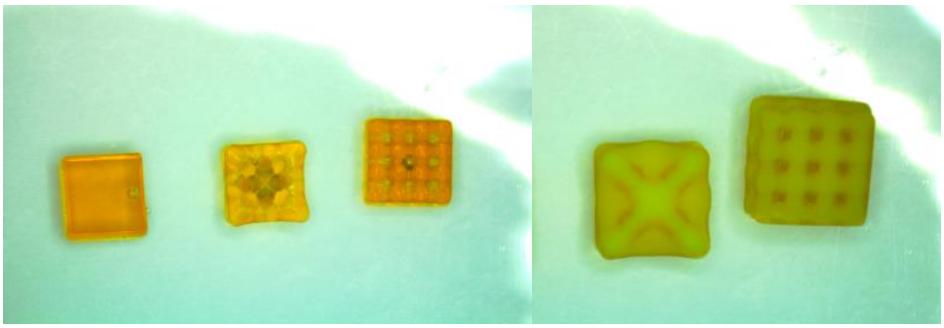

Figure 6-18 Swelling after one hour incubation in water.

Chapter 7

Conclusion and Future Work

This study used rapid prototyping (or also known as 3D printing system). A polyethylene glycol (PEG) based precursor was first designed and optimized to be printed using digital light processing (DLP) system.

Different hierarchical structures were printed with same relative density to be compared regarding their mechanical behavior and swelling properties. Also, the data was justified by modeling using ANSYS workbench. 4 different sets of samples with the same relative densities were modeled and studied for both single unit-cell and multi-unit cell structures.

In this context, three main structure were printed namely, 8.55 mm solid cube, 8.55 mm octet-truss structure, and 9.02 mm quad-truss structure (octet-truss and quad-truss structure have the same relative density). The solid structure was used as a control sample to specify the material's constants for subsequent use in the ANSYS calculations.

According to the simulation and experimental data, the octet-truss lattice structure has many advantages over the quad-truss structure:

- Although both structures show relatively the same Young's modulus, the octet-truss structure shows higher compressive strength and ultimate (failure) strain for multi-unit cell structures.
- Compressive strength of the multi-unit cell of the octet-truss structure is three times higher than that of the quad-truss structure.
- The ultimate (failure) strain at the failure point for multi-unit cell of the octet-truss structure is about four times higher than that of the quad-truss structure.
- The single unit-cell of the octet-truss structure, a stretch dominated structure, shows significantly higher elastic modulus and compressive strength.
- The elastic loading is more than 90% recoverable.

- The sample does not abruptly fail after initiation of a crack and it can also withstand subsequent higher loadings. Hence, even after reaching breaking point and crack initiation, the octet-truss structure remains uniform and can bear even more load.
- The octet-truss and quad-truss structures show rapid selling responses. However, the solid cube slowly swells and fails before reaching its fully swelled state (in less than 15 minutes).

In addition, the obtained ultimate (failure) strain data from our experiments is higher than 90% in simulation. Moreover, the obtained data from the experiment show higher than 80% similarity to acquired data from the simulation.

In the future, we will print smaller size dimensional structure in order to get ultralight, ultra-low density structures (with a wall thickness of less than 100μm). We expect that these structures show better properties than the structures constructed in this study.

References

1. Gao, W., et al., *The status, challenges, and future of additive manufacturing in engineering.* Computer-Aided Design, 2015.
2. Huang, Y., et al., *Additive Manufacturing: Current State, Future Potential, Gaps and Needs, and Recommendations.* Journal of Manufacturing Science and Engineering, 2015. 137(1): p. 014001.
3. Weller, C., R. Kleer, and F.T. Piller, *Economic implications of 3D printing: Market structure models in light of additive manufacturing revisited.* International Journal of Production Economics, 2015. 164: p. 43-56.
4. Melchels, F.P., J. Feijen, and D.W. Grijpma, *A review on stereolithography and its applications in biomedical engineering.* Biomaterials, 2010. 31(24): p. 6121-6130.
5. Huang, Y. and M.C. Leu, *Frontiers of Additive Manufacturing Research and Education.* 2014.
6. Reproduction, D.P.I. *3D Printing Basics: The Free Beginner's Guide*. 2014 May 2014 [cited 2015 Aug 21]; Available from: http://3dprintingindustry.com/3d-printing-basics-free-beginners-guide/.
7. Zhang, G.Q., et al. *Use of Industrial Robots in Additive Manufacturing-A Survey and Feasibility Study*. in *ISR/Robotik 2014; 41st International Symposium on Robotics; Proceedings of*. 2014. VDE.
8. Huang, S.H., et al., *Additive manufacturing and its societal impact: a literature review.* The International Journal of Advanced Manufacturing Technology, 2013. 67(5-8): p. 1191-1203.
9. Ashby, M., *The properties of foams and lattices.* Philosophical Transactions of the Royal Society of London A: Mathematical, Physical and Engineering Sciences, 2006. 364(1838): p. 15-30.

10. Zheng, X., et al., *Ultralight, ultrastiff mechanical metamaterials.* Science, 2014. 344(6190): p. 1373-1377.

11. Meza, L.R., S. Das, and J.R. Greer, *Strong, lightweight, and recoverable three-dimensional ceramic nanolattices.* Science, 2014. 345(6202): p. 1322-1326.

12. Schaedler, T.A., et al., *Ultralight metallic microlattices.* Science, 2011. 334(6058): p. 962-965.

13. Meza, L.R., et al., *Resilient 3D hierarchical architected metamaterials.* Proceedings of the National Academy of Sciences, 2015. 112(37): p. 11502-11507.

14. Sharma, P., *A Textbook of Production Technology: Manufacturing Processes*. 2007: S. Chand.

15. Parashar, B.N. and R. Mittal, *Elements of manufacturing processes*. 2002: PHI Learning Pvt. Ltd.

16. EngineersHandbook.com. *Manufacturing Methods*. 2004 [cited 2015 Oct 10]; Available from: http://engineershandbook.com/MfgMethods/.

17. Groover, M.P., *Fundamentals of modern manufacturing: materials processes, and systems*. 2007: John Wiley & Sons.

18. De Garmo, E.P., J.T. Black, and R.A. Kohser, *DeGarmo's materials and processes in manufacturing*. 2011: John Wiley & Sons.

19. Golden, A.P. and J. Tien, *Fabrication of microfluidic hydrogels using molded gelatin as a sacrificial element.* Lab Chip, 2007. 7(6): p. 720-725.

20. Freedman, D.H. *Layer by Layer*. 2011 [cited 2015 Sep 15]; Available from: http://www.technologyreview.com/featuredstory/426391/layer-by-layer/.

21. Wohlers, T., *additive manufacturing and 3D printing State of the industry.* Wohlers Associates, Fort Collins, CO, 2013.

22. Terry, W., *Additive manufacturing and 3D printing state of the industry*. 2012, Annual Worldwide Progress Report Wohlers Associstions.

23. Aviator. *Bae Systems Produces and Certifies 3D Printed Part for Use on BAE 146 JETLINER*. 2014 [cited 2015 Oct 22]; Available from: http://www.aviator.aero/press_releases/15570.

24. Bourell, D., et al., *A brief history of additive manufacturing and the 2009 roadmap for additive manufacturing: looking back and looking ahead.* Proceedings of RapidTech, 2009: p. 24-25.

25. Hockaday, L., et al., *Rapid 3D printing of anatomically accurate and mechanically heterogeneous aortic valve hydrogel scaffolds.* Biofabrication, 2012. 4(3): p. 035005.

26. Mannoor, M.S., et al., *3D printed bionic ears.* Nano letters, 2013. 13(6): p. 2634-2639.

27. MOLITCH-HOU, M. *Organovo Announces Its First 3D Bioprinted Kidney Tissue*. 2015 [cited 2015 Sep 28]; Available from: http://3dprintingindustry.com/2015/04/01/organovo-announces-its-first-3d-bioprinted-kidney-tissue/.

28. Directorate, N.S.T.M. *3D Printing: Food in Space*. 2013 July 28th, 2013 [cited 2015 Aug 07]; Available from: http://www.nasa.gov/directorates/spacetech/home/feature_3d_food.html.

29. MCDONAGH, C., *Boy's dreams come true as he receives 3d printed prosthetic arm*, in *Sunday Express* 2014.

30. Jessica. *Growing Objects – Algorithmic Sculptures*. 2014 [cited 2015 Aug 01]; Available from: http://n-e-r-v-o-u-s.com/blog/?p=6079.

31. Daicho, Y., et al., *Formation of three-dimensional carbon microstructures via two-photon microfabrication and microtransfer molding.* Optical Materials Express, 2013. 3(6): p. 875-883.

32. ORR, T. *ASTM International Proposes New 3D Printing Guidelines for Powder Bed Fusion Machines*. 2014 [cited 2015 Aug 14]; Available from: http://3dprint.com/13367/astm-international-standards/.

33. Sun, K., et al., *3D Printing of Interdigitated Li-Ion Microbattery Architectures.* Advanced Materials, 2013. 25(33): p. 4539-4543.

34. Luimstra, J. *This 3D Printing Extruder Can Print You a Nutella*. 2014 [cited 2015 Sep 11]; Available from: http://3dprinting.com/food/3d-printing-extruder-can-print-nutella/.

35. additively.com. *Overview over 3D printing technologies*. [cited 2015 Sep 06]; Available from: https://www.additively.com/en/learn-about/3d-printing-technologies.

36. Gibson, I., D.W. Rosen, and B. Stucker, *Additive manufacturing technologies*. 2010: Springer.

37. Venuvinod, P.K. and W. Ma, *Rapid prototyping: laser-based and other technologies*. 2013: Springer Science & Business Media.

38. Technology, L. *Laser Metal Deposition*. 2015 [cited 2015 Oct 01]; Available from: http://www.lpwtechnology.com/technical-information/laser-metal-deposition/.

39. Island, C. *Laser Powder Forming*. 2012 [cited 2015 Oct 01]; Available from: http://www.additive3d.com/lens.htm.

40. Gladstone, N. *Disadvantages of 3D Printers*. 2015 July 07, 2015 [cited 2015 Sep 21]; Available from: http://www.ehow.com/facts_7652991_disadvantages-3d-printers.html.

41. Deshpande, V., M. Ashby, and N. Fleck, *Foam topology: bending versus stretching dominated architectures.* Acta Materialia, 2001. 49(6): p. 1035-1040.

42. Gibson, L.J. and M.F. Ashby, *Cellular solids: structure and properties*. 1997: Cambridge university press.

43. Maxwell, J.C., *L. on the calculation of the equilibrium and stiffness of frames.* The London, Edinburgh, and Dublin Philosophical Magazine and Journal of Science, 1864. 27(182): p. 294-299.

44. Deshpande, V.S., N.A. Fleck, and M.F. Ashby, *Effective properties of the octet-truss lattice material.* Journal of the Mechanics and Physics of Solids, 2001. 49(8): p. 1747-1769.

45. Calladine, C.R., *Theory of shell structures*. 1989: Cambridge University Press.

46. Meza, L.R., S. Das, and J.R. Greer, *Supplementary Materials for Strong, lightweight, and recoverable three-dimensional ceramic nanolattices.* Science, 2014. 345(6202): p. 1322-1326.

47. Johnston, S.R., et al. *Analysis of mesostructure unit cells comprised of octet-truss structures*. in *Proceedings of the The Seventeenth Solid Freeform Fabrication Symposium Austin, TX*. 2006.

48. Renton, J.D., *Elastic beams and frames*. 2002: Elsevier.

49. Pan, Y., C. Zhou, and Y. Chen, *A fast mask projection Stereolithography process for fabricating digital models in minutes.* Journal of Manufacturing Science and Engineering, 2012. 134(5): p. 051011.

50. McNaught, A.D. and A.D. McNaught, *Compendium of chemical terminology*. Vol. 1669. 1997: Blackwell Science Oxford.

51. Thermo Scientific, I., *Thermo scientific pierce crosslinking technical handbook.* Retrieved June, 2009. 10: p. 2010.

52. Lee, H. and N.X. Fang, *Micro 3D printing using a digital projector and its application in the study of soft materials mechanics.* Journal of visualized experiments: JoVE, 2012(69).

Biographical Information

Hakan Arslan received his B.S. degree in Mechanical Engineering from Gazi University, Turkey, in 2009. After finishing his B.S., he accomplished several internships in different areas, which are QA/QC Engineering, Manufacturing Engineering, and R&D Engineering. He completed his M.S. degree at the University of Texas at Arlington in Mechanical Engineering in Fall 2015. His areas of interest includes optimization of 3D printed structures.